LAWRENCE
LIVERMORE
NATIONAL
LABORATORY

LLNL-TR-637432

Reaction of Gold with Indium Below 50°C: Radius Loss Delta R and Standard Deviation Sigma of Soldered 4 mil Wires at 100 Years Predicted from Measured Delta R and Sigma at 30 Years.

W. J. Siekhaus, J. Go, M. Biener, S. A. Jensen, M. A. Havstad, J. Cheng, C. A. Hrousis, Z. Chiba, M. E. Oldaker, W. McLean

May 24, 2013

Disclaimer

This work performed under the auspices of the U.S. Department of Energy by Lawrence Livermore National Laboratory under Contract DE-AC52-07NA27344.

Reaction of gold with indium below 50°C: radius loss ΔR and standard deviation ∑ of soldered 4 mil wires at 100 years predicted from measured ΔR and ∑ at 30 years.

Wigbert J. Siekhaus, Monika Biener, Jackson Go, Margaret "Peggy" Kervin
Steven Jensen, Mark Havstad, James Cheng,
Zoher Chiba, Constantine Hrousis, William McLean, Mark Oldaker.

Abstract

Gold wire radius loss (ΔR±∑) measured in metallurgical sections of Pb-Sn-In solder mounds of a set of headers with 4 mil gold wires at age 30 years together with a careful reconstruction of their temperature/time history prove that the long-term gold-indium reaction at low temperatures is controlled by diffusion of indium from the solder through the $AuIn_2$ reaction product layer to the gold surface, i.e. proportional to the square root of time, ΔR=~√time. The dependence of the standard deviation data scatter ∑ on radius loss ΔR, i.e. ∑=f(ΔR), is deduced from data sets of 1.5 mil gold wires together with this small set of measurements of 4 mil wires. These two data sets are really insufficient to have complete confidence in the soundness of the function ∑=f(ΔR). Its validity is somewhat "vetted" by showing its consistency with the ΔR±∑, ΔR±2∑, ΔR±3∑ values observed during the approximately 30 year life of 1.5 mil headers held at higher temperatures and hence larger ΔR loss. That larger ΔR loss is comparable to the ΔR loss expected over 100 years for the 4mil wire sets analyzed here at their lower temperature. Hence the values of ∑=f(ΔR) are added to Δr=~√time to predict ΔR±∑, ΔR±2∑, ΔR±3∑ for 4 mil wires up to an age of 100 years at temperatures they experienced during their first 30 years. ΔR±3∑ values at age 100 years are predicted to be less than 24μm.

Diffusion control of the gold loss reaction, ΔR=~√time, implies that the reaction product layer is integer, without cracks that would permit rapid transport of indium. That requirement is readily fulfilled in un-constrained planar geometry where the growing product layer can expand without resistance. However, in circular geometry relevant here for gold loss of 4 mil wires, an existing reaction product layer ($AuIn_2$) is constantly expanded by the next layer of $AuIn_2$ formed below it at the gold surface. Hence cracks can develop unless the mechanical properties of $AuIn_2$ and of the surrounding solder are such that the solder can con tinuously plastically deform the existing $AuIn_2$ layer to prevent cracking or to "heal" any cracks that form. Nano-indentation measurements show that $AuIn_2$ is not brittle, but that its hardness and elastic modulus are higher than those of gold and of the solder components. The radial metallurgical sections reveal that locally "healing" does not always succeed since the remaining gold wire frequently does not have circular geometry, but rather has often "flat spots" where more rapid gold loss has occurred and thicker $AuIn_2$ has formed above the flat spots. Hence while "on average" the gold loss is diffusion controlled, proportional to √time, locally there are clearly spots where the gold loss and $AuIn_2$ formation is greater. The strength of the surrounding solder needed to heal the expanding $AuIn_2$ layer is weakest where the wire exits from the solder mound. Axial sections through the center-line of wires indicate that at the exit point enhanced reaction may indeed occur.

Content

I) Introduction

The reaction of gold with indium in Pb/Sn/In solder mounds forming gold-indide ($AuIn_2$) initially proceeds linearly with time [1] and that functional dependence has been used at LLNL and elsewhere [2] to conservatively predict gold loss with the equation ((gold radius loss ΔR=1.45*10^10*exp(-7990/T°K)*time(month). The reaction changes, however, to square root of time dependence with increasing gold loss [3], clearly detectable at elevated temperatures, where data can be acquired in relatively short time. (Gold radius loss ΔR=1.51*10^7*exp(-5245.3/T°K)*√time(month)). Reliably documenting this change-over to square-root of time dependence at low temperature (substantially less than 50°C) requires experiments that last over many years.

Those reliable long time/low temperature data have not been available until now making it necessary to rely on the linear time dependence for conservative long-time predictions of critical components.

For the reaction of gold with indium alone equations that incorporate both the linear and the square root of time dependence have been developed by Millares [4] based on short-time experiments at temperatures at and above 50°C.

In this report we have for the first time accurate temperature history data for a set of headers exposed to low temperatures for about 30 years and a sufficient number of header solder mound sections to determine a well defined average gold wire radius loss ΔR together with a value of the standard deviation data scatter $\sum$ around ΔR deduced from a normal distribution fit to the data. We reconstruct the day to day temperature history of samples that have spent at a variety of locations approximately thirty years at temperatures varying between 7 °C and 40°C and show that this temperature history applied to the linear model of reference [1] overestimates the gold loss by up to a factor 2.8, while, in contrast, the square root of time model of reference [3] predicts the measured gold loss within the experimental error.

---

[1] Reaction Between Thin Gold Wires and Pb-Sn-In Solder, Part A. W. J. Siekhaus,
[2] Gold-Indium Intermetallic Compounds: Properties and Growth Rates. J. E. Jellison, http://nepp.nasa.gov/DocUploads/5858DEF9-1650-445E-AB08C869805951CA/Gold%20Indium%20Intermetallic%20Compounds%20Properties%20and%20Growth%20Rates.pdf
[3] Reaction Between Thin Gold Wires And Pb-Sn-In Solder, Part C. W. J. Siekhaus, LLNL-TR-469341.
[4] Reaction/Diffusion In The Au-In System. Millares, M. Pieraggi, B., Solid State Ionics, **63-65** 1993, 575-580.

II) Data

II.1) Gold radius loss measurements

To generate the most information from the limited set of headers, particularly to establish the data scatter ∑ around the mean radius loss ΔR, both solder mounds of five sets of headers were sectioned radially, and some headers were also subsequently sectioned axially, as shown in figure 1.

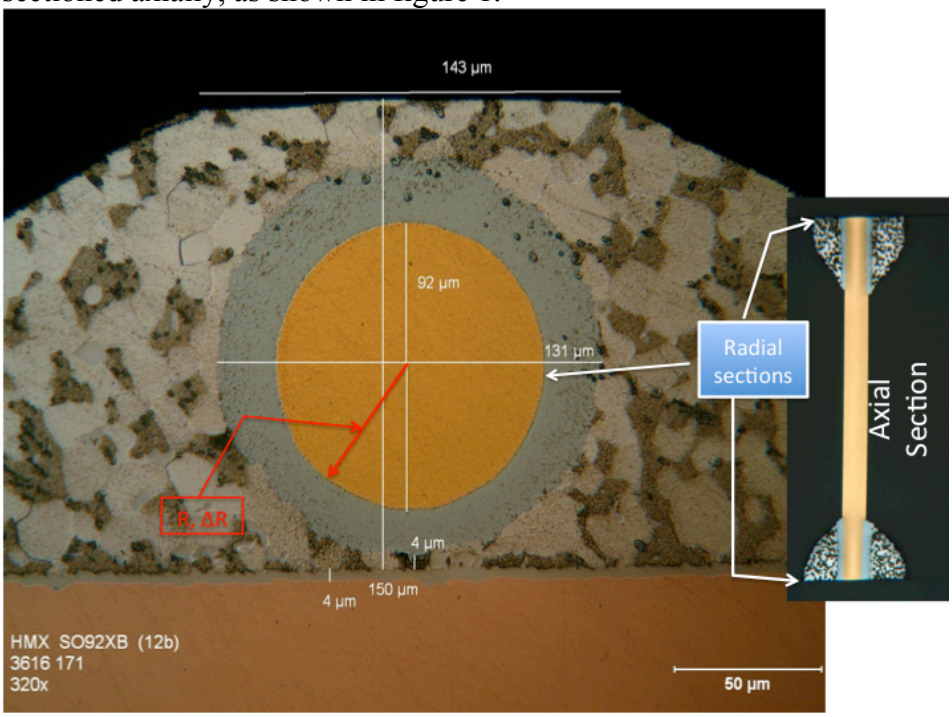

Figure 1. Images of a radial and an axial section of one header.

One set of headers had been held "bare" in "Storage" at a controlled temperature of 20°C, while the other sets identified in the table below by numbers 33 to 94 had a widely varying temperature history discussed below. Table I lists the mean value of the gold radius loss ΔR together with the data scatter ∑ deduced from a normal distribution function fit to the data sets.

Identification	Time, Month	Average Radius Loss ΔR, µm	Data Scatter Standard Deviation ∑, µm	Data Scatter % of ΔR
Storage	333.5	4.685	± 0.25	± 5
33	352.5	5.675	± 0.95	± 16
48	336.0	6.175	± 1.49	± 24
76	336.0	7.613	± 0.95	± 12.5
94	336.0	6.050	± 0.65	± 11

Table I. Measured average gold radius loss ΔR and data scatter of each data set.

II.2) Time/temperature history of the data sets.

While the headers identified as "Storage" in table 1 were held at a controlled constant temperature of 20°C, the other headers were located during their life history in bunkers at different locations, for various lengths of time, and in addition were contained in various configurations, with an added heat source. Figure 2 indicates the steps required to create an accurate time/temperature history for the wide variety of storage locations, named for simplicity north, south, east, west…. Accurate records were used that document each set's time at a particular storage location together with its specific configuration (i.e. bare, in device, in container, in delivery vehicle…). The configuration changed frequently during the storage time at a location, changing thereby the set's temperature. Each location has an "external" temperature record, sometimes provided by NOAA (the National Oceanic and Atmospheric Administration). The bunker's thermal properties change the seasonal approximately sinusoidal external temperature profile (blue trace in figure 2) to an internal approximately sinusoidal profile (red trace in figure 2): the internal sinusoidal amplitude is smaller, its mean temperature shifts "up" by $\Delta T1$, and its phase shifts by Φ radians. The presence of a heat source increases the set's temperature by $\Delta T2$ whose magnitude depends on the particular configuration it is held in. The bunker's and the configurational temperature effects were applied to create a day-by-day history of each header set. The rate of gold loss $\Delta R(time)$ is governed by an equation of the form $\Delta R = B * \exp(-(A/T)) * f(time)$. Figure 3 demonstrates why it is necessary to use the actual sinusoidal temperature history rather than the average temperature to determine gold loss.

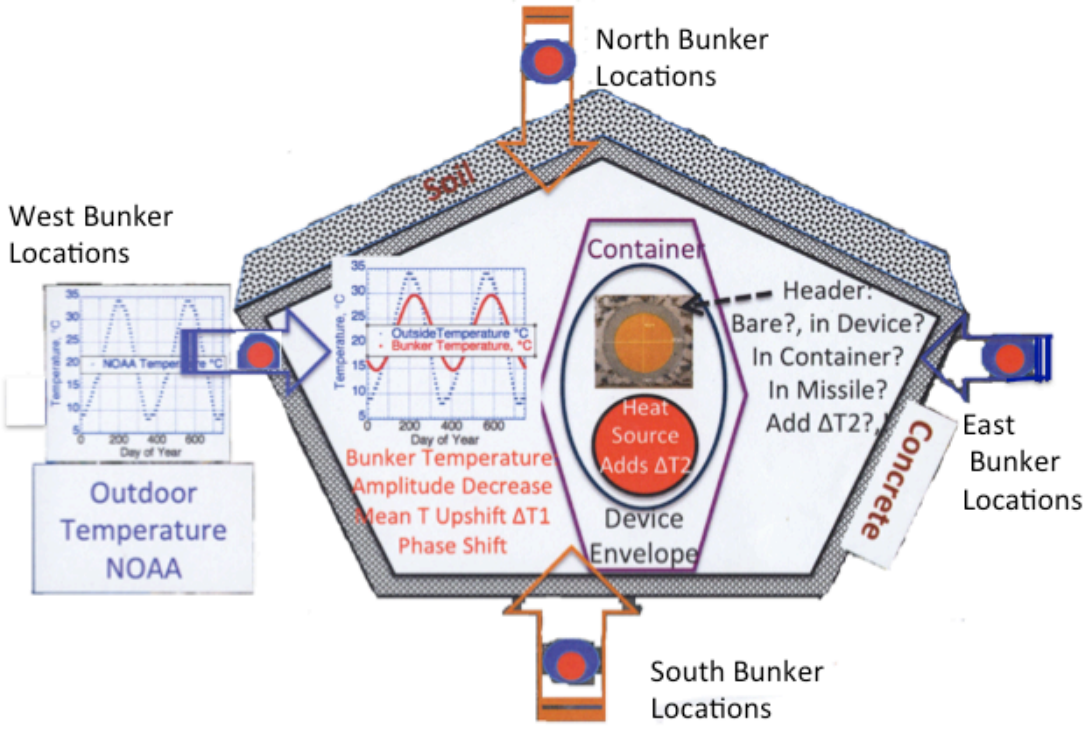

Figure 2. Bunker and storage configuration effects on header set's temperature.

The rate of gold loss depends exponentially on activation energy and temperature; hence the gold loss during the time where the sinusoidal temperature is above average temperature is much larger than that during the time below average.

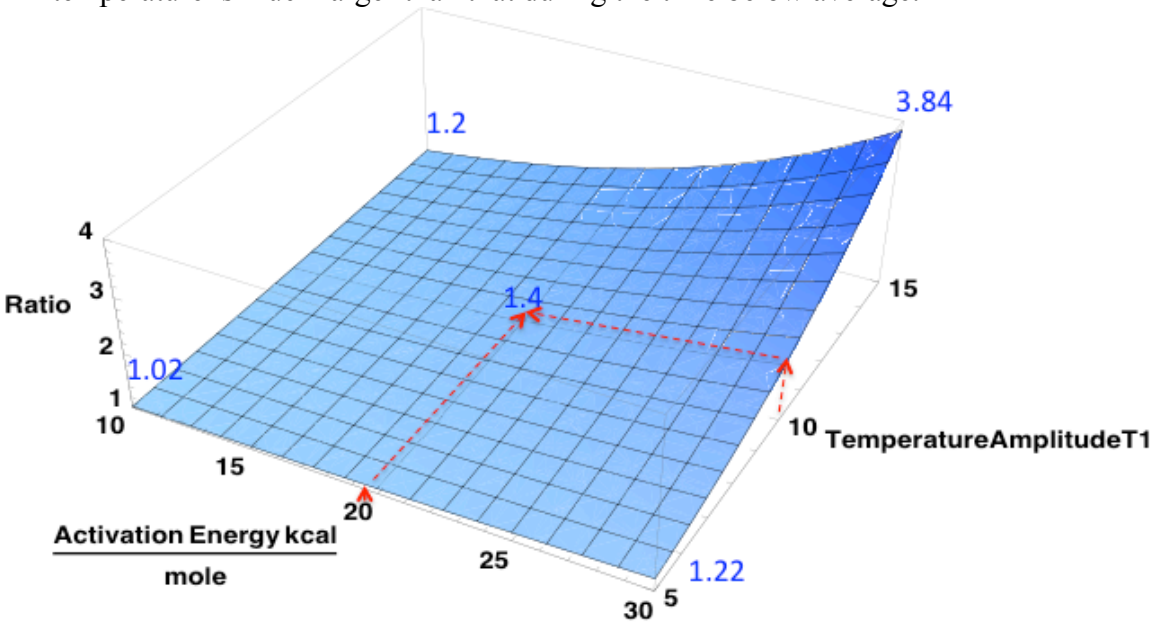

Figure 3. Ratio = (reaction product formed over one year using the actual sinusoidal temperature/reaction product formed using the mean temperature) for a reaction described by Constant*exp(-Activation Energy/Temperature) as a function of activation energy and temperature amplitude. The mean temperature is 283°K.

Figure 3 shows that for a chemical reaction with a "typical" activation energy of 20kcal/mole and a sinusoidal amplitude of 10°K around a mean temperature of 283°K the gold loss is under-estimated by 40% if the average temperature is used. For a reaction with an activation energy of 80kcal/mole the reaction product formation would be under-estimated by a factor 19.
Unfortunately there exist at the time of this report only for one bunker at a northern location a reliable set of external and internal temperature measurements from which a bunker's effect on temperature can be deduced, displayed in figure 4.
Figure 4 shows first that temperature measurements were done correctly at this location: The sinusoidal fit (blue line) to the external temperatures (blue dots) agrees closely with NOAA data (brownish dots). At the other (southern) location where data are available the temperature measurements were not done correctly, there the blue fit line deviates substantially from the NOAA data.

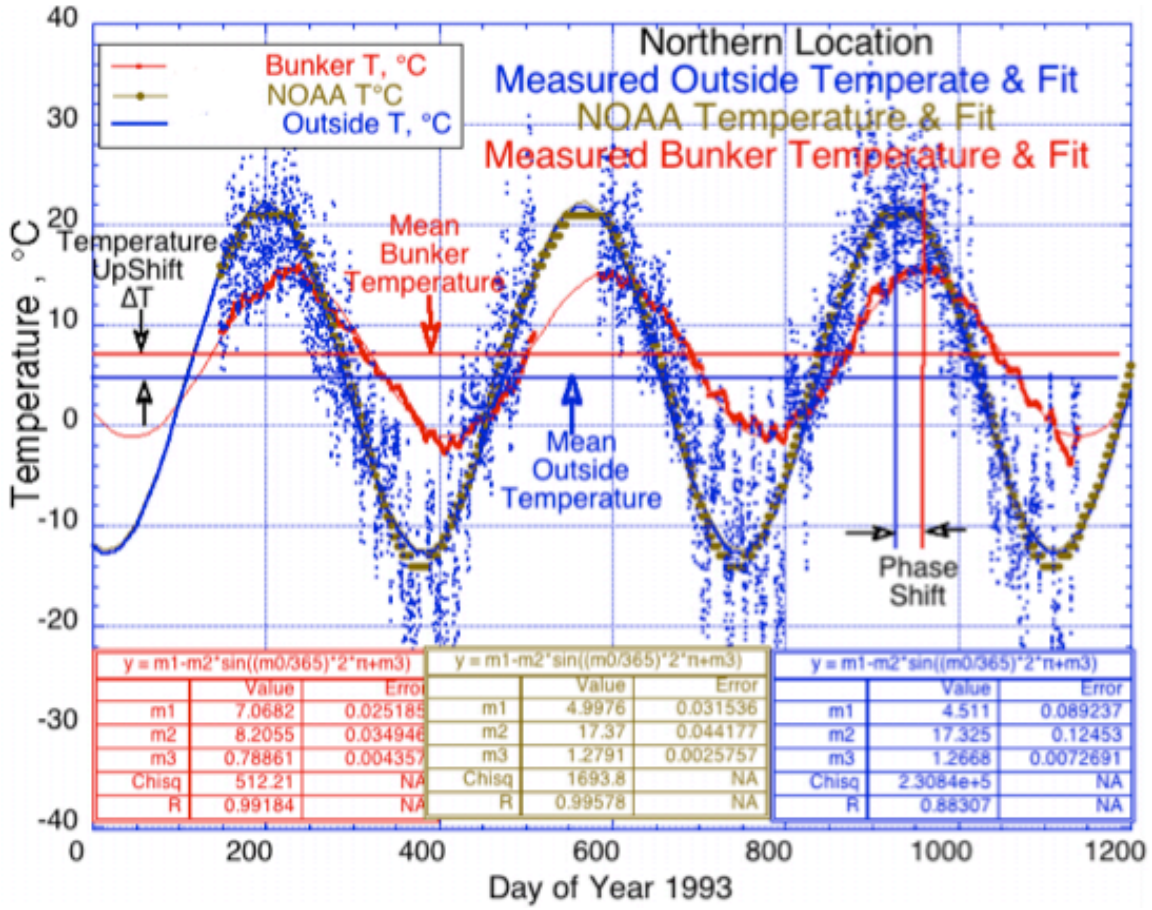

Figure 4. Daily external (blue) and internal (red) temperatures measured at a northern location and NOAA average external temperatures (brownish), together with (in boxes of the same color at the bottom of the figure) the parameters of sinusoidal fits to the data.

Figure 4 further illustrates how a bunker changes external temperature into internal temperature: the large *daily* external temperature variations (blue dots) are damped out by the thermal inertia of the bunker so that their internal amplitude (in red) is reduced a few degrees. Figure 3 demonstrates that only a small error occurs if one uses the average of that small temperature fluctuation when calculating gold loss. That average of the internal temperature is represented by the sinusoidal fit (red line). The boxes at the bottom of the graph show the parameters of the fit equation:

$$\text{Temperature (°C)} = m1 - m2 \cdot \sin\left(\left(\frac{m0}{365}\right) \cdot 2\pi + m3\right).$$

Here m1 is the average temperature, m2 the amplitude of the sine, m0 is the day of the year, and m3 the phase of the sine in radians. The phase of the fit changes from m3=1.2668 (external, blue) to .78861 (internal, red), a phase shift of $\Phi = 0.48$ radians, equivalent to approximately 28 days. The average "upshift" in temperature is $\Delta T1 = 2.6$°C (from m1=4.511 (blue) to m1=7.0682 (red)) and the external amplitude m2=17.325°C (blue) is reduced by about a factor two to internal amplitude m2=8.2055°C (red). The sinusoidal fits with a single sine component are NOT a perfect fit, as can be seen in the fit to the NOAA data: the lowest temperatures are slightly underestimated.

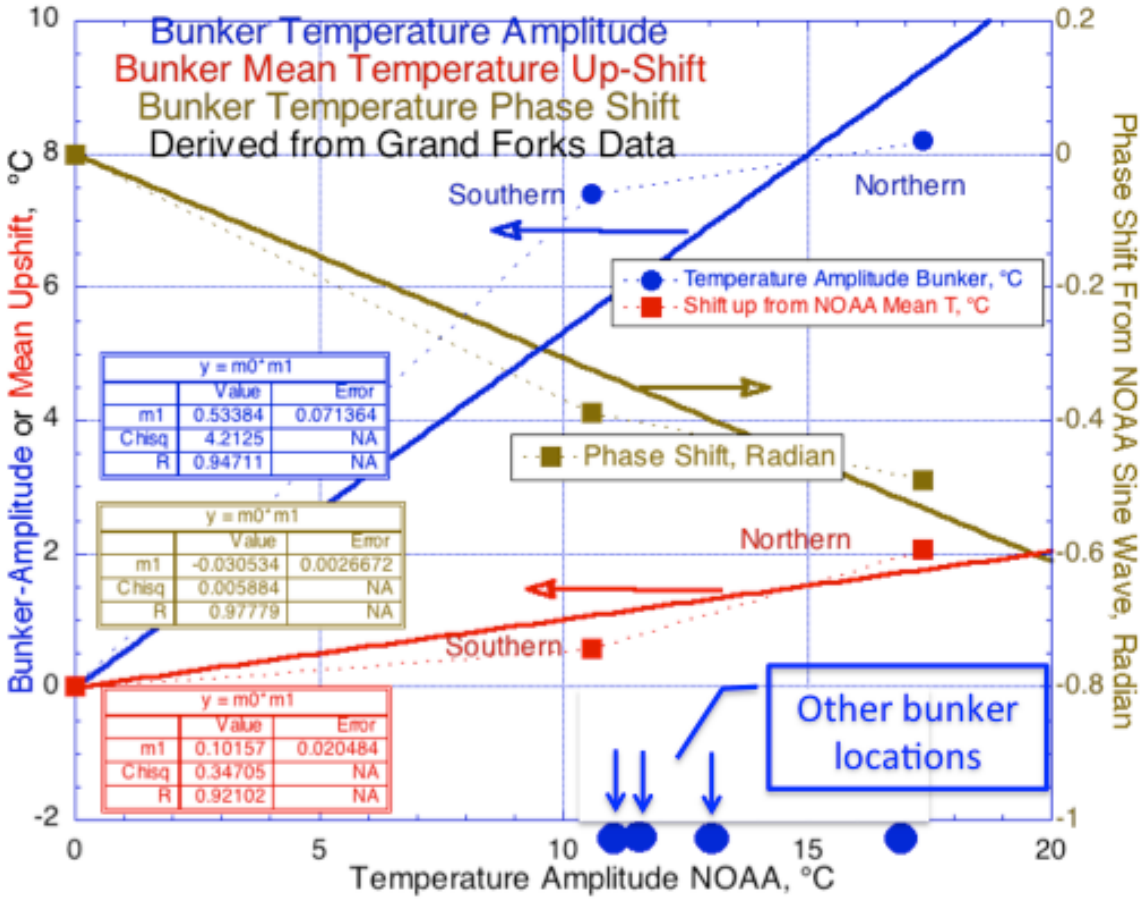

Figure 5. Estimation of bunker temperature amplitude, upshift and phase shift based on the assumption that these bunker effects vary linearly with external temperature amplitude.

Since no other external/internal temperature measurements are available at other locations, the following assumptions were made to estimate the bunker effect there: 1) the bunker effect is zero if there is constant external temperature year-round; 2) the bunker effect varies linearly with external temperature amplitude. With these assumptions amplitude changes, temperature upshifts and phase shifts can be estimated from figure 5.

The linear fit equations shown in boxes in the left of figure 5 are applied in the calculation of daily temperature at all bunker locations. Figure 5 includes data from the incorrectly measured southern location after applying a correction to those data.

The temperature increase $\Delta T2$ due to the presence of a heat source has been the subject of recent measurements and modeling calculations that have been leading to differing result. Here it is chosen to be 9°C when the headers were held in an additional storage/transportation container, and 5°C otherwise.

III) Test of reaction models

III.1) The linear reaction model

$$\Delta R(\mu m) = 1.45 * 10^{10} * \exp(-7990/T(^{\circ}K)) * \text{time (month)} \qquad (1)$$

The time/temperature history data described above were used for all sets in the linear reaction model, only two examples of which are shown here in figures 6 and 7.

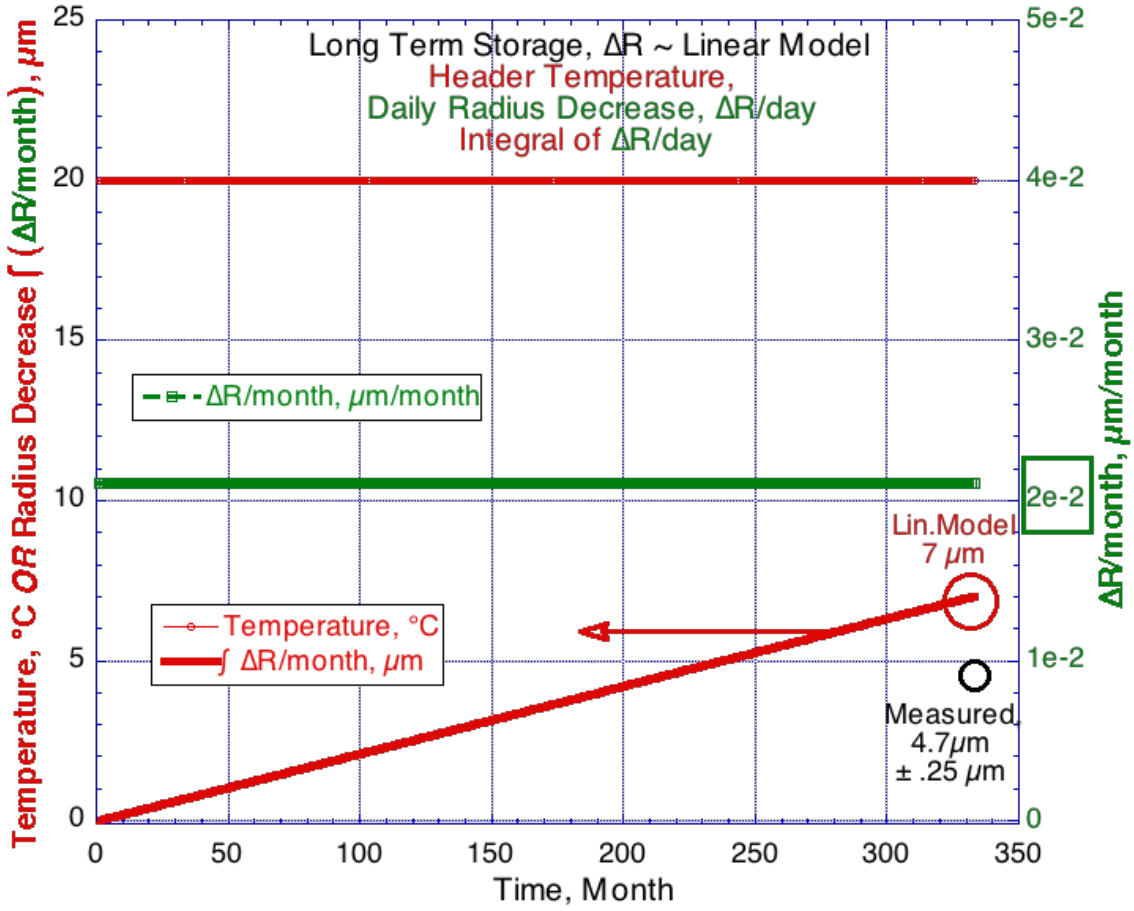

Figure 6. The header temperature (upper red line, °C), and the calculated monthly radius decrease (green line, ΔR/month, μm/month) and its integral ΔR (lower red line, ΔR, μm) of the header set labeled "storage" using the reaction rate equation (1).

Both figure 6 and figure 7 show the discrepancy between the calculated radius loss (red circle) and the radius loss (black circle) measured at ~ 10^4 days and demonstrate clearly that the linear model overestimates the rate of reaction and hence cannot be used for long term predictions of gold loss at long exposure times.

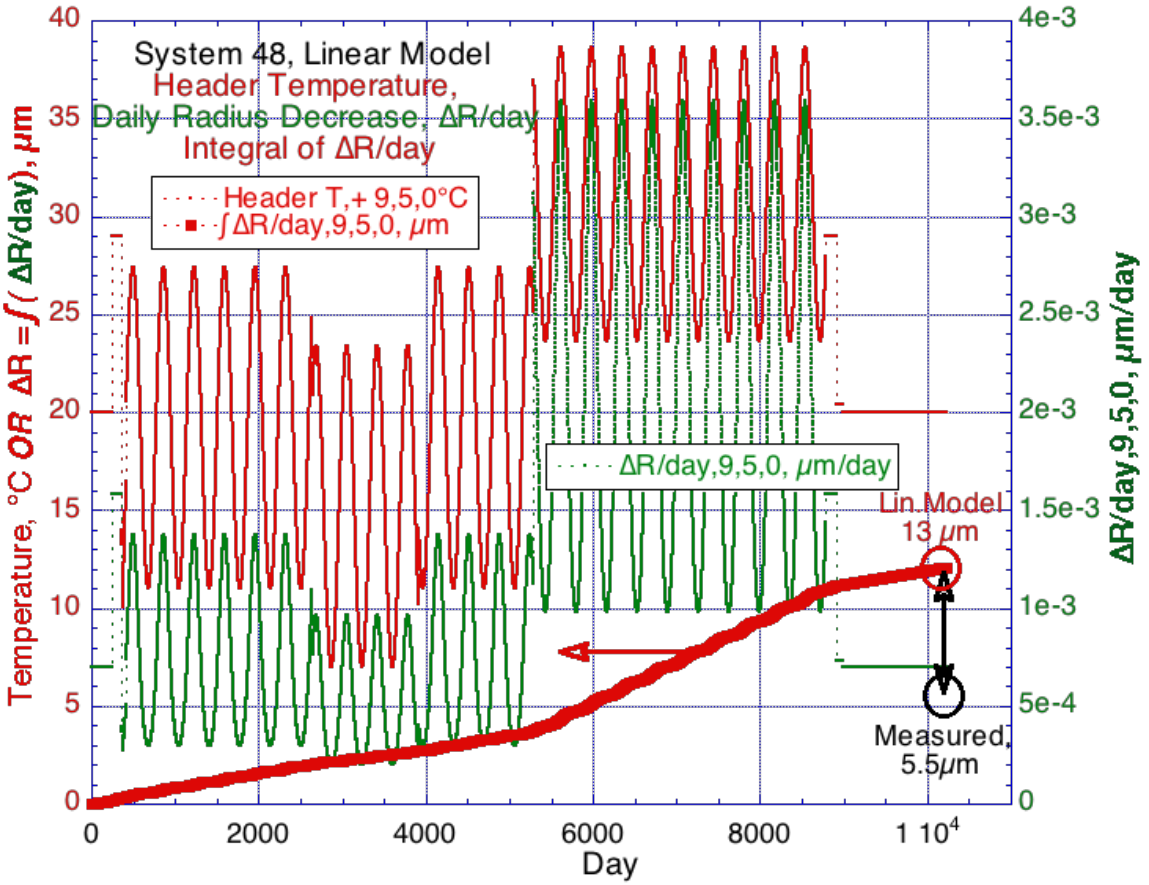

Figure 7. The header temperature (upper thin red line, °C), and the calculated daily radius decrease (green line, ΔR/day, μm/day) and its integral ΔR (lower fat red line, ΔR, μm) of the header labeled "48" using the reaction rate equation (1).

System	Storage LTS	33	48	76	94
ΔR measured, μm	4.7	5.5	5.7	5.7	6
ΔR predicted, μm - Linear model	7	13	14	16	13.25
Too high by a factor:	1.5	2.4	2.5	2.8	2.2

Table II. Comparison of the radius loss ΔR predicted by the linear model with the measured radius loss.

In Table II computed radius losses for all header sets are shown to exceed measured losses by as much as a factor 2.8. The linear reaction model of equation (1) clearly can NOT be applied to predict radius loss for long term exposure at low temperature.

III.2) Test of the diffusion-control reaction model.

$$\Delta R(\mu m) = 1.505 * 10^{7} * \exp(-5245/T(^{\circ}K)) * \sqrt{time}\ (\sqrt{month}) \qquad (2)$$

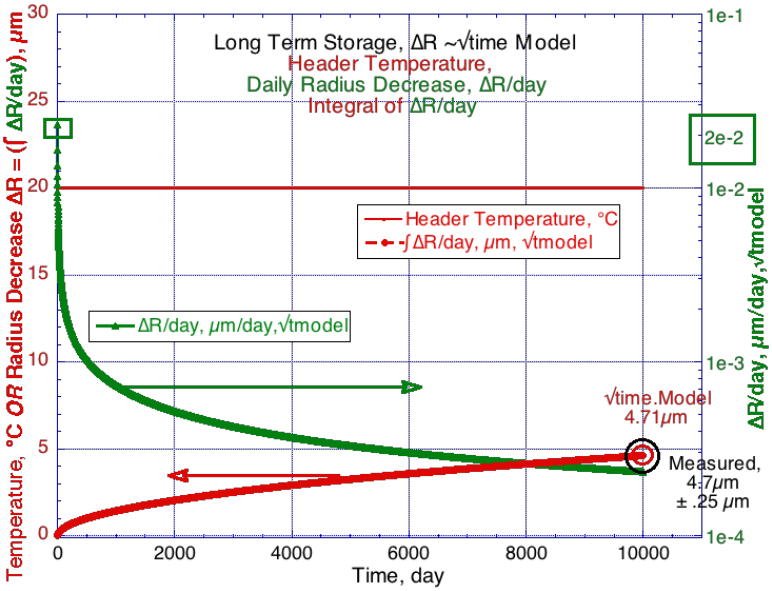

Figure 8. The header temperature (thin upper red line, °C), and the calculated daily radius decrease (green line, ΔR/day, μm/day) and its time integral ΔR (lower red line, ΔR, μm) of the header set "storage" using the reaction rate equation (2).

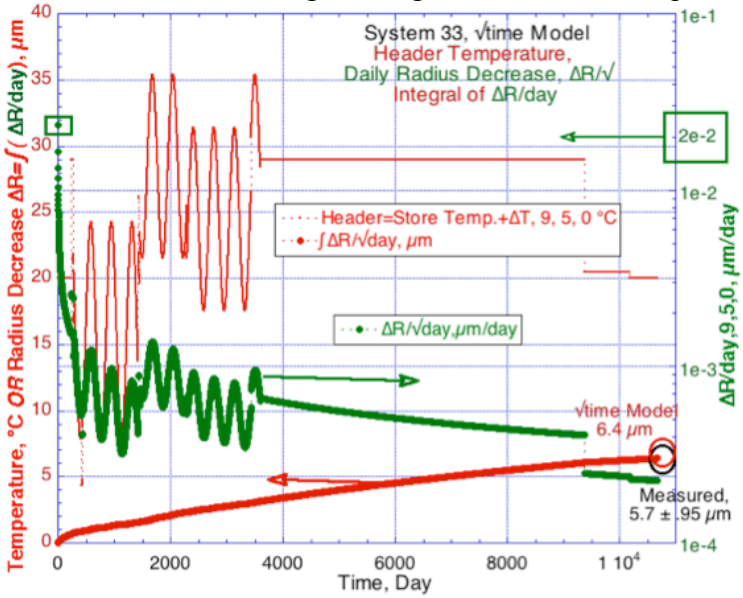

Figure 9. The header temperature (upper thin red line, °C), the calculated daily radius decrease (green line, ΔR/day, μm/day) and its time integral ΔR (lower fat red line, ΔR, μm) of the header labeled "33" using the reaction rate equation (2).

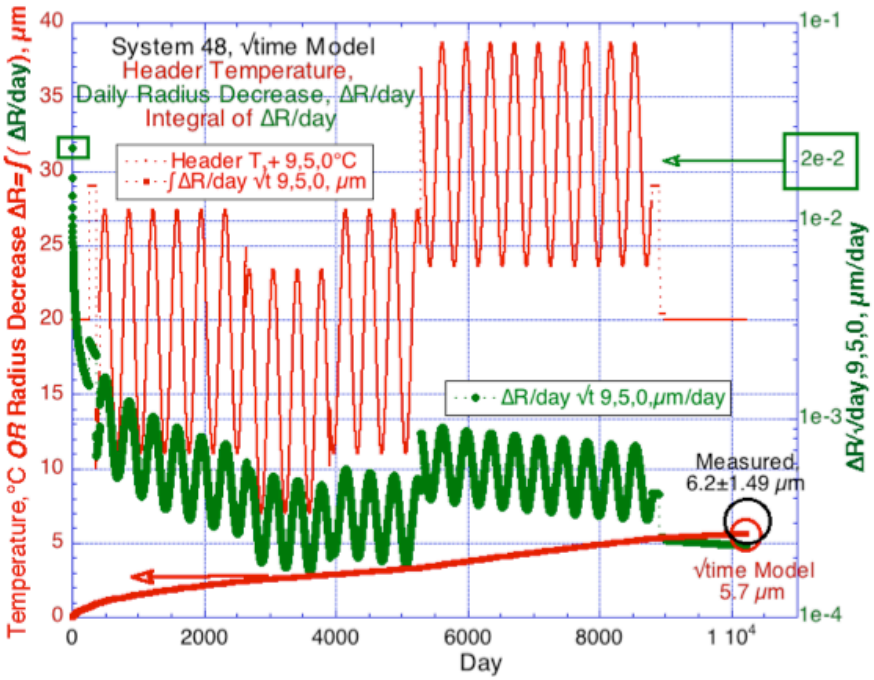

Figure 10. The header temperature (upper thin red line, °C), and the calculated daily radius decrease (green line, ΔR/day, μm/day) and its time integral ΔR (lower fat red line, ΔR, μm) of the header labeled "48" using the reaction rate equation (2).

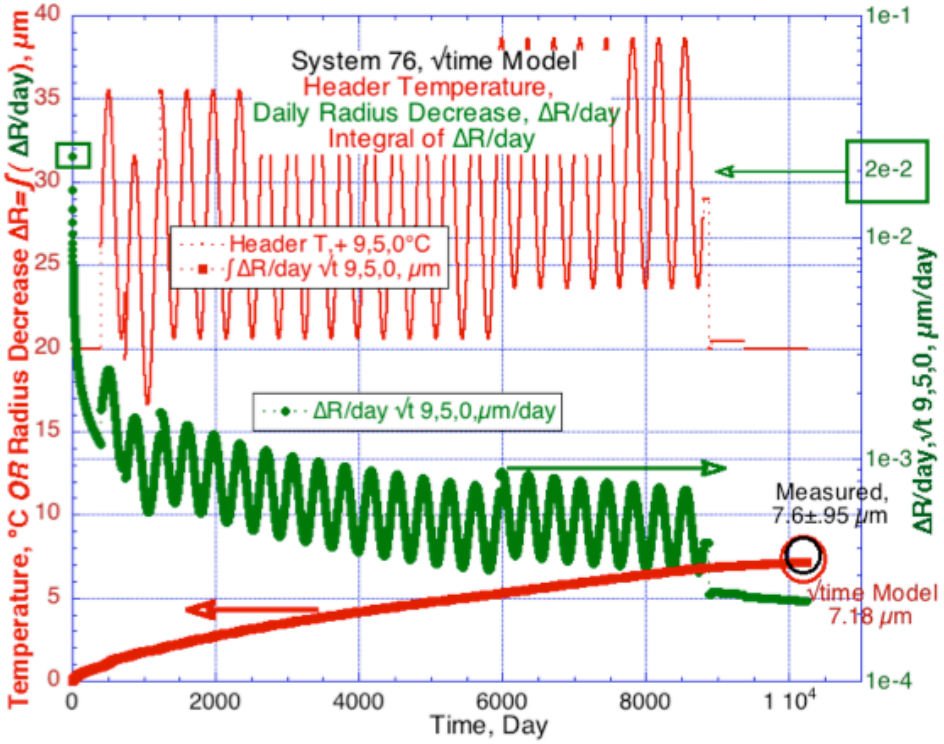

Figure 11. The header temperature (upper thin red line, °C), and the calculated daily radius decrease (green line, ΔR/day, μm/day) and its time integral ΔR (lower fat red line, ΔR, μm) of the header set labeled "76" using the reaction rate equation (2).

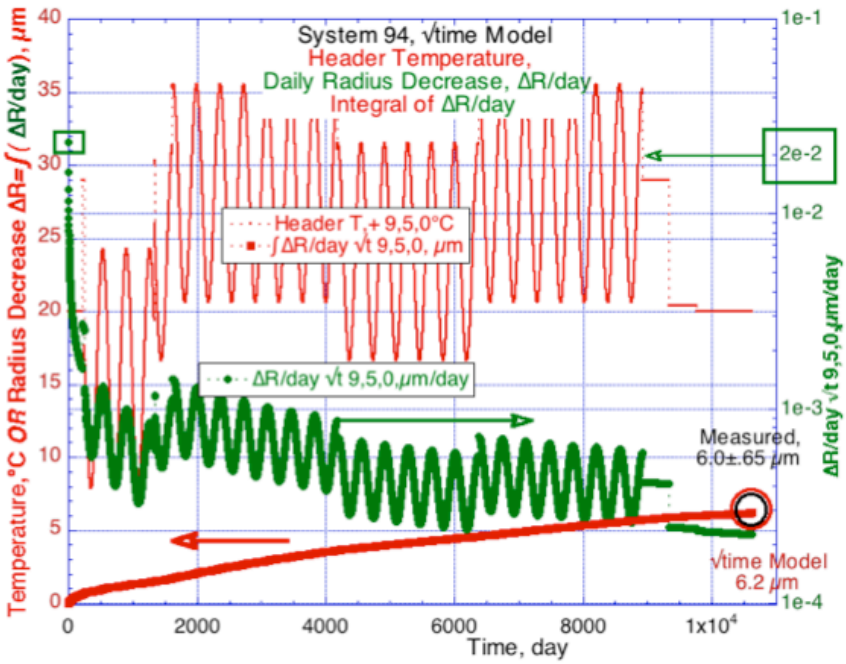

Figure 12. The header temperature (upper thin red line, °C), and the daily radius decrease (green line, ΔR/day, μm/day) and its time integral ΔR (lower fat red line, ΔR, μm) of the header labeled "94" using the reaction rate equation (2).

System	Storage LTS	33	48	76	94
ΔR Measured, μm	4.68±.25 ±5%	5.7±.95 ±16%	6.2±1.5 ±24%	7.6±.95 ±12.5%	6.05±.65 ±11%
ΔR Predicted, μm -√time model	4.7	6.4	5.7	7.18	6.2
Compare: Within ? %, Less than experimen-tal ± error !!	1%	+12%	-11%	-6%	+2.5%

Table III. Comparison of the radius loss ΔR predicted by the non-linear model (~√time) with the measured radius loss.

Figures 8 to 12 display and table III summarizes the excellent agreement between the radius loss (red circles) calculated by equation (2) and the measured radius loss (black circles), both at constant temperature and at widely varying temperatures. This close agreement demonstrates clearly that the non-linear model (~√time) correctly describes the rate of reaction during long-term exposure at low temperatures and can be used with confidence to predict the radius loss for times beyond the time where these measurements were made. Table III summarizes the results and demonstrates that the difference between measured and calculated radius loss is always well with in the data scatter ∑ of the experimental data for exposures with widely varying temperature history. That fact implies that the activation energy of this rate equation is correct.

IV) The calculated *average* gold radius loss ΔR at age 100 years of set "76" by quadrupling its time/temperature history.

Section III.2 demonstrates that gold radius loss ΔR in PbSnIn solder mounds is controlled by diffusion of indium through the reaction product ($AuIn_2$) layer and is correctly described for long term exposure at temperatures below 50 °C by the equation (2) using the actual time/temperature history. As an example, in figure 13 the results of radius loss calculations are shown that occur during approximately 100 years by adding the sinusoidal part of the time/temperature history of the set "76" (figure 11) three more times. Set "76" experienced the highest temperatures during its life.

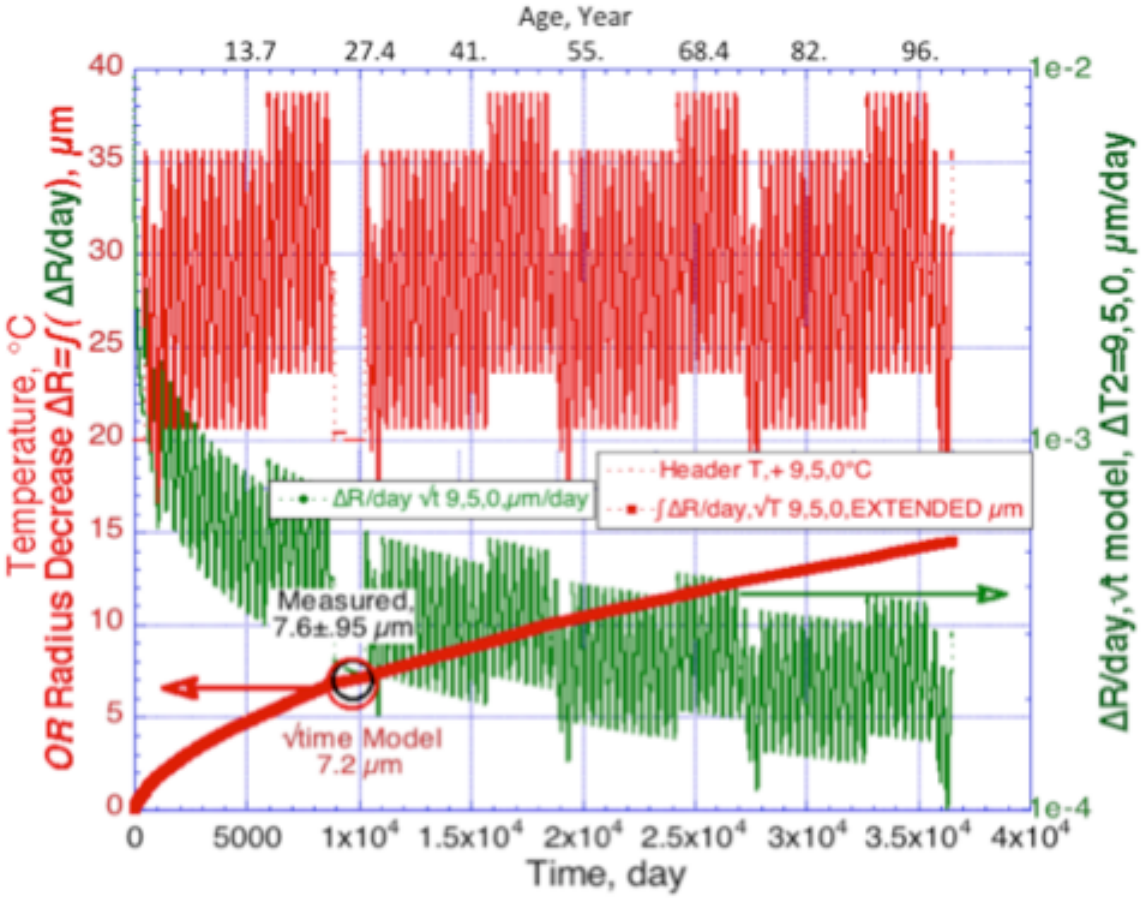

Figure 13. The radius loss ΔR (thick red line) of a 4 mil gold bridge-wire expected during approximately 100 years while experiencing the sinusoidal temperature history of the set "76" three more times.

The result is a radius loss of approximately 14.5 μm, about twice as much seen above in figure 11 for the set "76" at age 30 years, as expected for a reaction proportional to the square root of time.

V. Estimate of the dependence ∑=f(ΔR) of the standard deviation data scatter ∑ on the average radius loss ΔR.

For critical components it is equally important to know the data scatter ±∑, ±2∑, ±3∑ around the average gold radius loss ΔR. The magnitude of statistical variations ∑ of chemical reactions depends most likely both on the extent of the reaction (here ΔR) and the temperature at which the reaction occurred. Hence to make an estimate it would be ideal to have several sets of samples that have been aged at constant temperatures in the range of interest for very long times and with sufficient numbers that a cumulative distribution function could be fit revealing both Δr and ∑ with good confidence. Unfortunately there are now known only sets of 1.5 mil wires aged at 22.5 and 34.6 degree centigrade for 159 and 123.5 month, respectively, and the 4 mil wire sets discussed here.

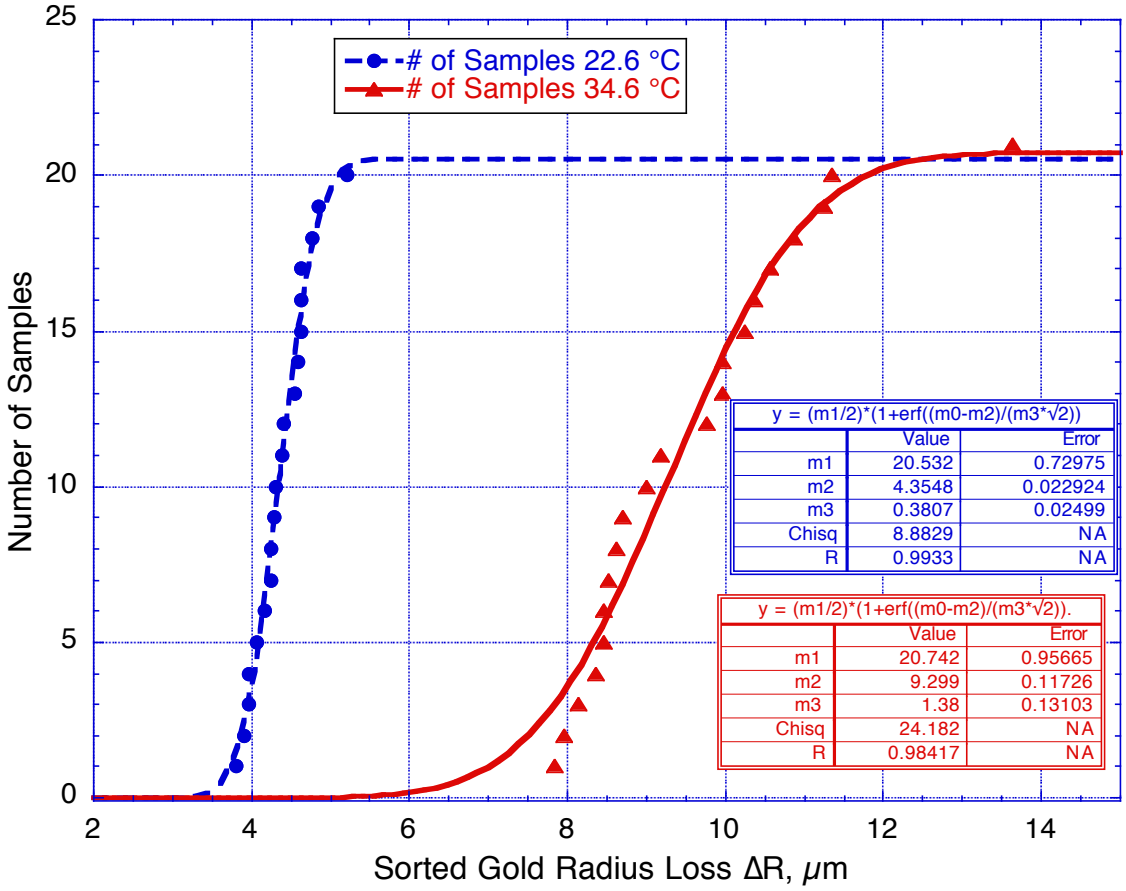

Figure 14. The Gaussian ("normal") cumulative distribution function fit to the 1.5 mil data sets (see fit parameters m2=$\Delta R_{average}$ and m3=∑ in the boxes).

In figure 14 the number of samples are plotted versus the ΔR losses of 1.5 mil gold wires at 22.6°C and 34.6°C sorted in ascending order, and the cumulative distribution function (CDF) of the normal distribution is fitted to the plots. The figure demonstrates that the data scatter of the gold-indium reaction can be fit reasonably well by a "normal"

distribution function. In figure 15 the ∑ values from figure 14 for 1.5 mil wires and those of table I for 4 mil wires are plotted versus ΔR. There is a lot of scatter in the ∑- values, they do not nicely fall onto a straight line, but neither should one expect that, since they are taken at various temperatures. Nevertheless, it is clear that the data scatter ∑ increases with increasing ΔR, and to first order, ∑ appears to increase linearly with ΔR. Two linear fits are shown in figure 15: in black a fit to ALL data,

$$\sum_{average} = 0.16^* \Delta R \qquad (3)$$

and in red a fit only to the largest ∑ of table I for set "48"

$$\sum_{max} = 0.24^* \Delta R. \qquad (4)$$

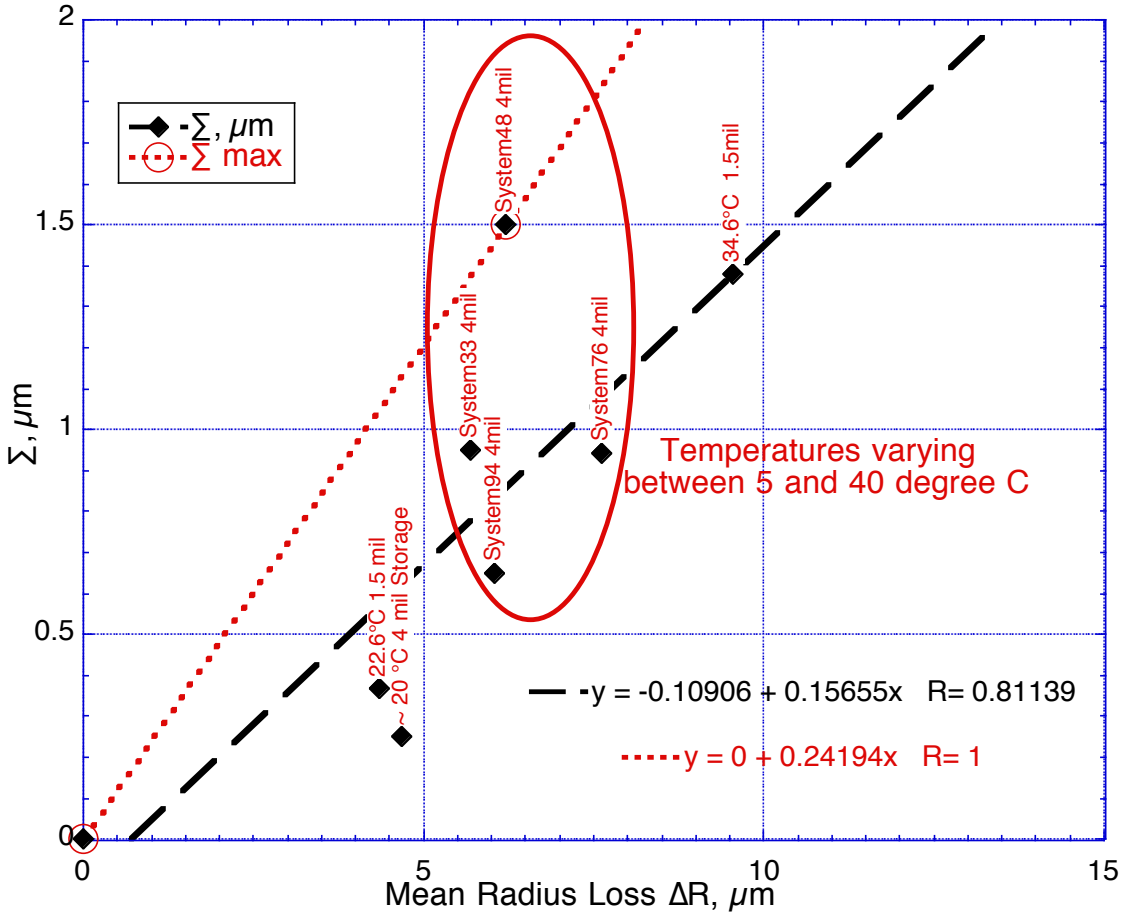

Figure 15. The standard deviation ∑ as a function of mean gold wire radius loss ΔR of two sets of 1.5 mil wires, and the 4 mil wire sets of table I.

VI. "Vetting" of the functional dependence ∑= f(ΔR) of part V) using the "PeggyDataSet".

It is clear that more data sets at constant temperatures and at longer exposure time in the range of interest here are highly desirable, but for now the two linear dependences of ∑ on R will be used, first to check whether they are consistent with the data scatter observed over 30 years on 1.5 mill wire data (named "Peggy") at higher average temperatures than the sets of figure 1. Thereafter equation 4 ($\sum_{max} = 0.24^*\Delta R$) will be applied to *predict* the future data scatter for 4 mil wires. In figure 16 equation (2) is fitted to the ΔR values of the "Peggy" data set (thin blue line, called "PeggyFit"). Then

equation (4) ($\sum_{max}$ = 0.24*ΔR) is added to or subtracted from the PeggyFit and the results are plotted as medium thick purple lines labeled (PeggyFit+1∑max) and (PeggyFit-1∑max). Equation 4 added twice to or subtracted twice from PeggyFit results in the thick red lines labeled (PeggyFit+2∑max) and (PeggyFit-2∑max). There are 69 data points in the PeggySet of which 35 (=52%) lie within the lines PeggyFit±∑max and 65 (=94.2%) lie within the lines PeggyFit±2∑max. A data set with a perfect normal distribution would have 68.27% and 95.45%, respectively, between those lines. 4 data points (=5.8%) lie beyond the red PeggyFit±2∑max lines versus 4.55% expected in a normal distribution. No data point lies close to or beyond the PeggyFit±3∑max lines (nor drawn).

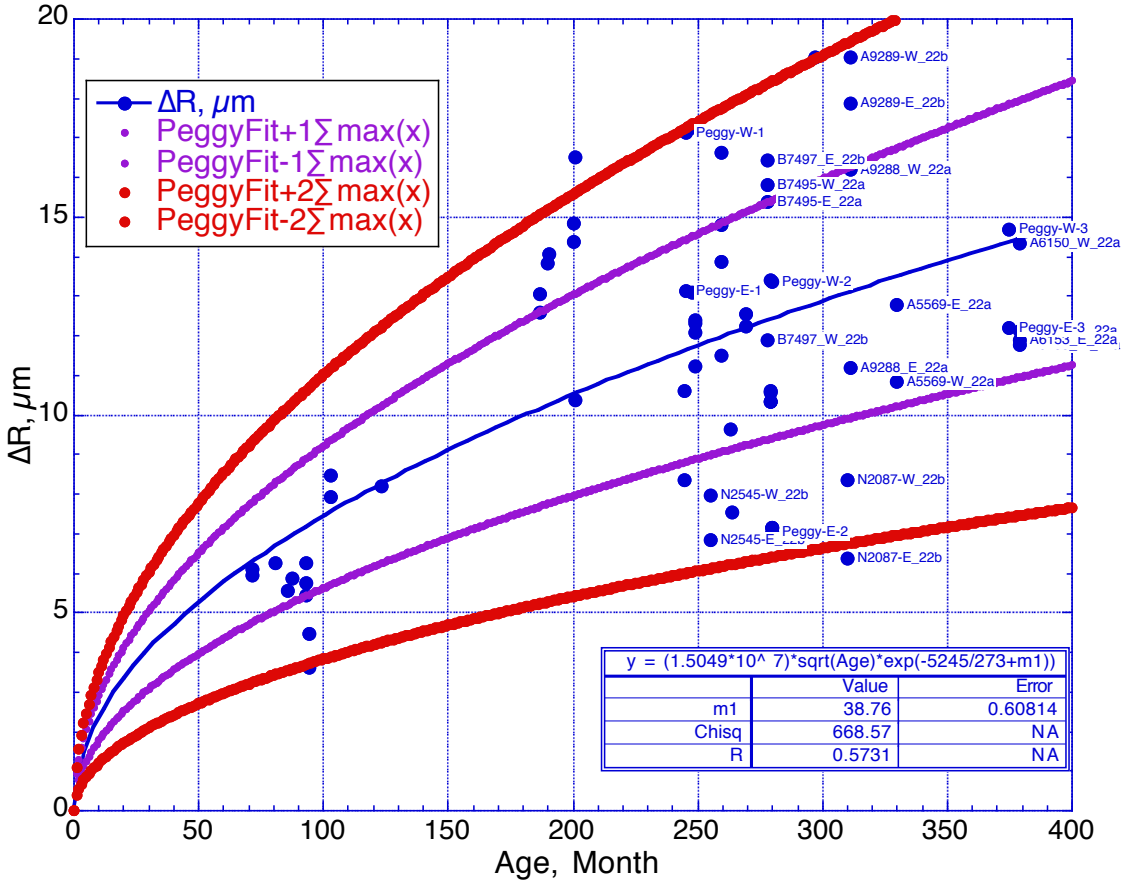

Figure 16. Fit (thin blue line) of equation (2) (see box) to ΔR, and ±∑ (thicker purple line) and ±2∑ (very thick red line) curves generated by adding the values ±$\sum_{max}$(R)=.24*ΔR (equation 4) and ±2*$\sum_{max}$(R)=2*.24*ΔR, respectively, to equation (2). The fit of equation (2) results in an average temperature of 38.76°C during the life of the PeggySet.

One should not expect that the total number of data points acquired over many years from samples whose time/temperature history is not completely known behaves exactly like a data set with normal distribution. It is, however, comforting to observe that ΔR±∑ predictions based on equation (2) together with equation (4) {$\sum_{max}$ = 0.24*ΔR} are close to ΔR values observed experimentally over thirty years on a header set and that all data lie below the ΔR±3∑ lines.

In contrast, in figure 17, where equation (3) {$\sum_{average}$= 0.16*ΔR)} is used to add ±$\sum_{average}$, ±2*$\sum_{average}$, ±3*$\sum_{average}$ to the equation (2) fit to ΔR values of the PeggySet, a few data points do lie at or even beyond the brown PeggyFit±3*$\sum_{average\ lines}$.
For that reason the prediction of data scatter for the 4 mil data set in part VII will be based on using equation (2) to generate the average radius loss ΔR, and equation (4) {$\sum_{max}$= 0.24*ΔR} to generate ∑s.

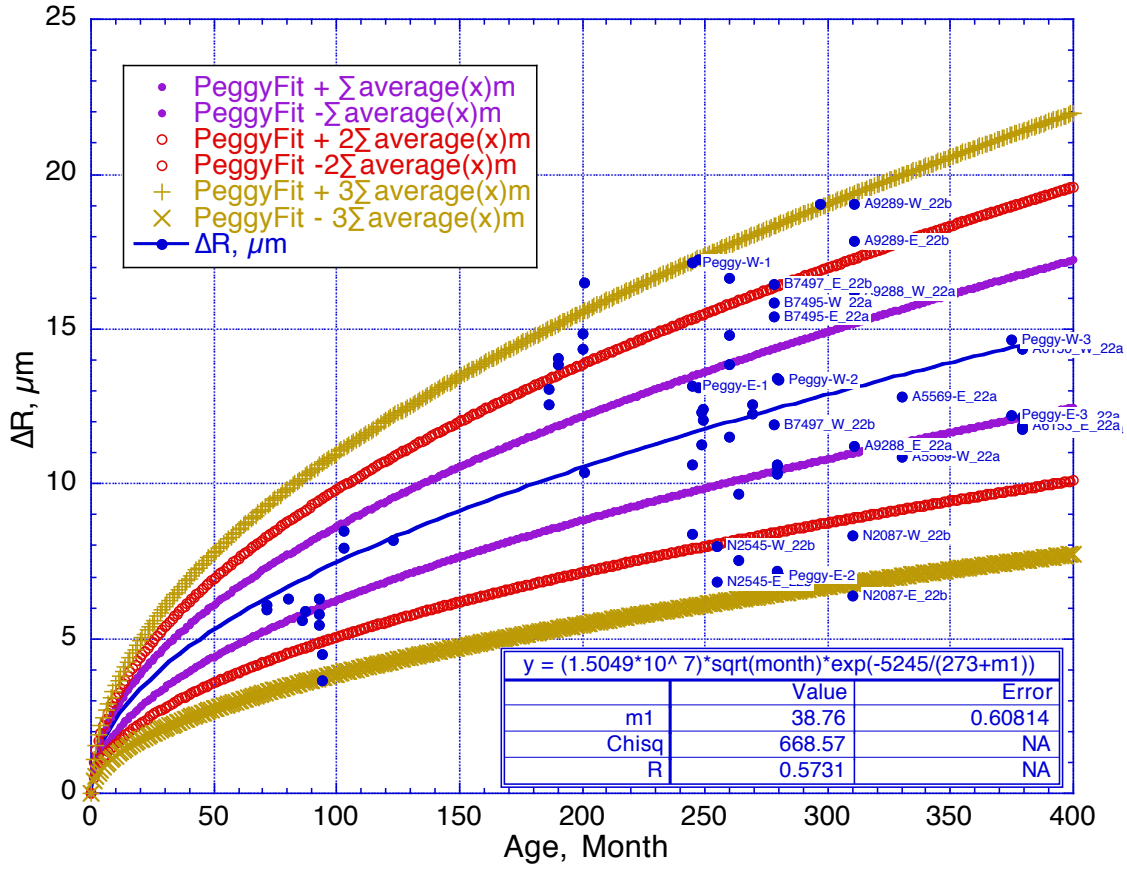

Figure 17. Fit (thin blue line) of equation (2) (see box) to the PeggySet and ±∑ (thicker purple line) and ±2∑ (even thicker red line) and ±3∑ (very thick brown line) curves generated by adding $\sum_{average}$(R)=0.16 *ΔR (equation 3), 2*$\sum_{average}$(R)=2*.16*ΔR and 3$\sum_{average}$(R)=3*.16*ΔR, respectively, to equation (2) with T= (273+38.76)°K.

VII) The *average* gold radius loss ΔR and its *standard deviations* $\pm\sum_{max}$, $\pm 2\sum_{max}$, $\pm 3\sum_{max}$ for the 4 mil wire set up to age 100 years predicted using equations (2) and (4).

The data set "76" experienced the highest temperatures. To calculate ΔR values equivalent to those seen in figure 13 where "76"s actual temperature history was quadrupled to reach age 100 years, i.e. ΔR= ~ 14µm, an average temperature of 28 °C was used in equation (2) go generate the ΔR curve in Figure 18. The final ΔR value of 14µm predicted here for 4mil header sets after 100 years at ~28°C is about the same as the experimentally observed ΔR value reached in the PeggySet (see figures 16 and 17) after about 30 years at ~ 38°C. In figure 16 the $\pm\sum_{max}$ curves represent the scatter of the experimentally observed ΔR values reasonably well, 94.2% lie within the $\pm 2\sum_{max}$ curves, and the remaining data are very close to $\pm 2\sum_{max}$ curves, far away from $\pm 3\sum_{max}$ curves. It is thus sensible to assume that data sets "33" to "94" will show the same behavior as they age to 100 years. Hence such sets should with high confidence generate experimental ΔR values that lie within the $\Delta R \pm 3\sum_{max}$ curves shown in figure 18.

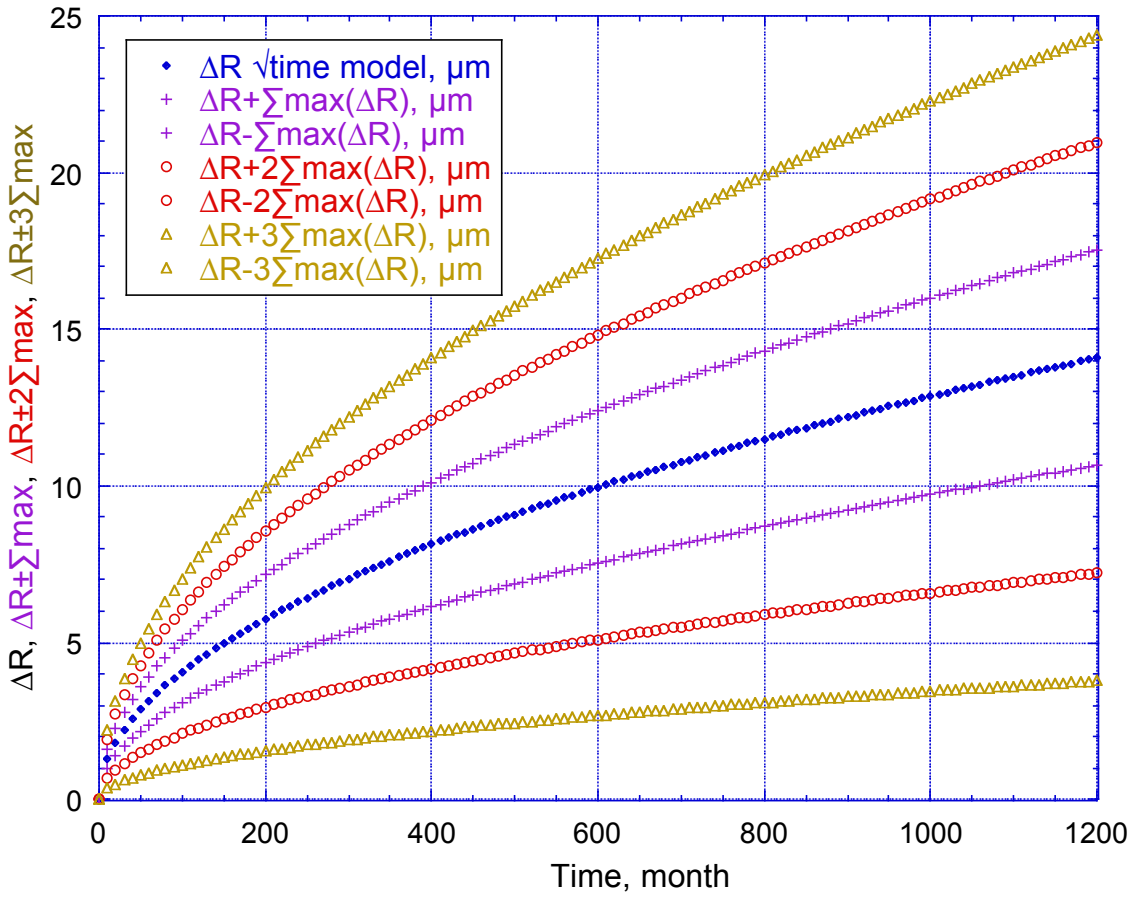

Figure 18. Equation (2) with T= (273+28)°K (blue circles) and $\pm\sum_{max}$ (purple crosses) and $\pm 2\sum_{max}$ (red circles) and $\pm 3\sum_{max}$ (brown triangles) curves generated by adding $\sum_{max}(R)=.242*\Delta R$ (equation 4), $2*\sum_{max}(R)=2*.242*\Delta R$ and $3\sum_{max}(R)=3*.242*\Delta R$, respectively, to equation (2).

VIII) Effects of circular geometry on the integrity of the $AuIn_2$ layer, and hence on diffusion-controlled gold radius loss.

VIII.1) Description of the effects.

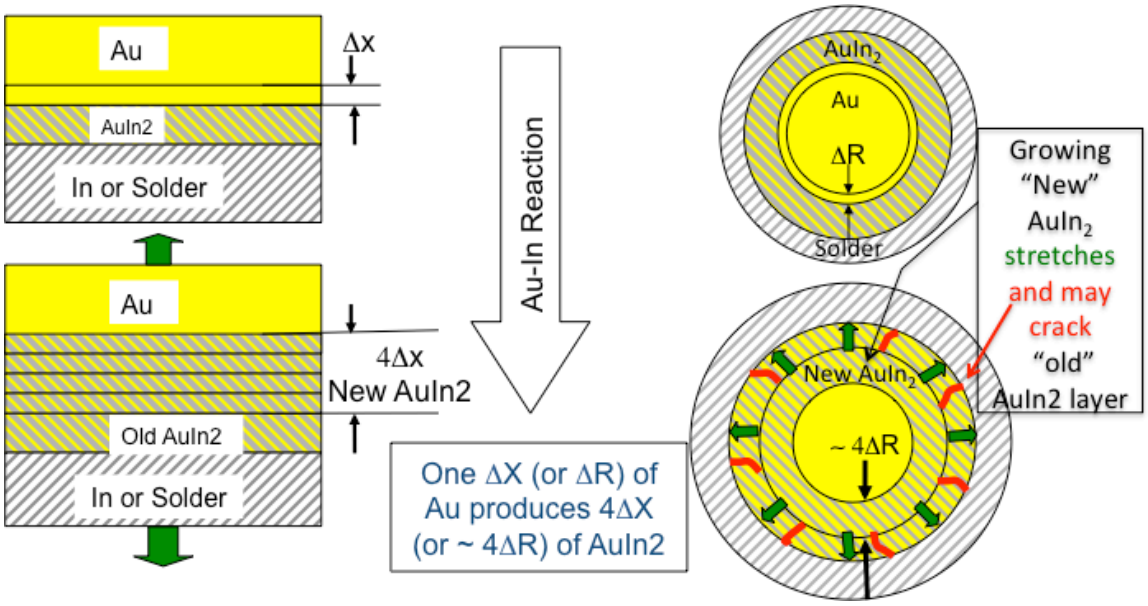

Figure 19. Left: In planar geometry the growing $AuIn_2$ easily pushes gold and indium/solder material apart. Right: in circular geometry the next growing $AuIn_2$ layer stretches and potentially cracks the former $AuIn_2$ layer.

Diffusion control of indium through the growing $AuIn_2$ layer required for the applicability of equation (2) is only assured if the layer is integer, without cracks. That is probable in un-constrained planar geometry where $AuIn_2$ growth simply pushes the faces of gold and of the source of indium (either solder or pure indium) further apart (green arrows in the left part of figure 19). Equation (2) is partially, and Millares's equation [3] is wholly, derived from $AuIn_2$ growth in planar geometry. In cylindrical geometry, however, new $AuIn_2$ growth deforms and may crack the existing $AuIn_2$ layer, thus producing rapid diffusion paths, unless the mechanical properties of $AuIn_2$ and solder are such that $AuIn_2$ is pliable enough and the surrounding solder is strong enough to plastically deform the existing $AuIn_2$ layer to avoid forming cracks or to heal the cracks that do form. The mechanical properties of $AuIn_2$ have been described as "friable" with "Diamond Pyramid Hardness Units" between 55 and 77 (=.54 -> .76 GPa) [2]. Here we use nano-indentation to measure the mechanical properties of $AuIn_2$ "as grown" and of the constituents of the solder, i.e. Pb/In and Sn/In.

VIII.2) Morphology of $AuIn_2$, and of Pb/In and Sn/In "grains" in an axial section of a solder mound, and hardness and elastic modulus measurements of Au, $AuIn_2$, and of Pb/In and Sn/In "grains".

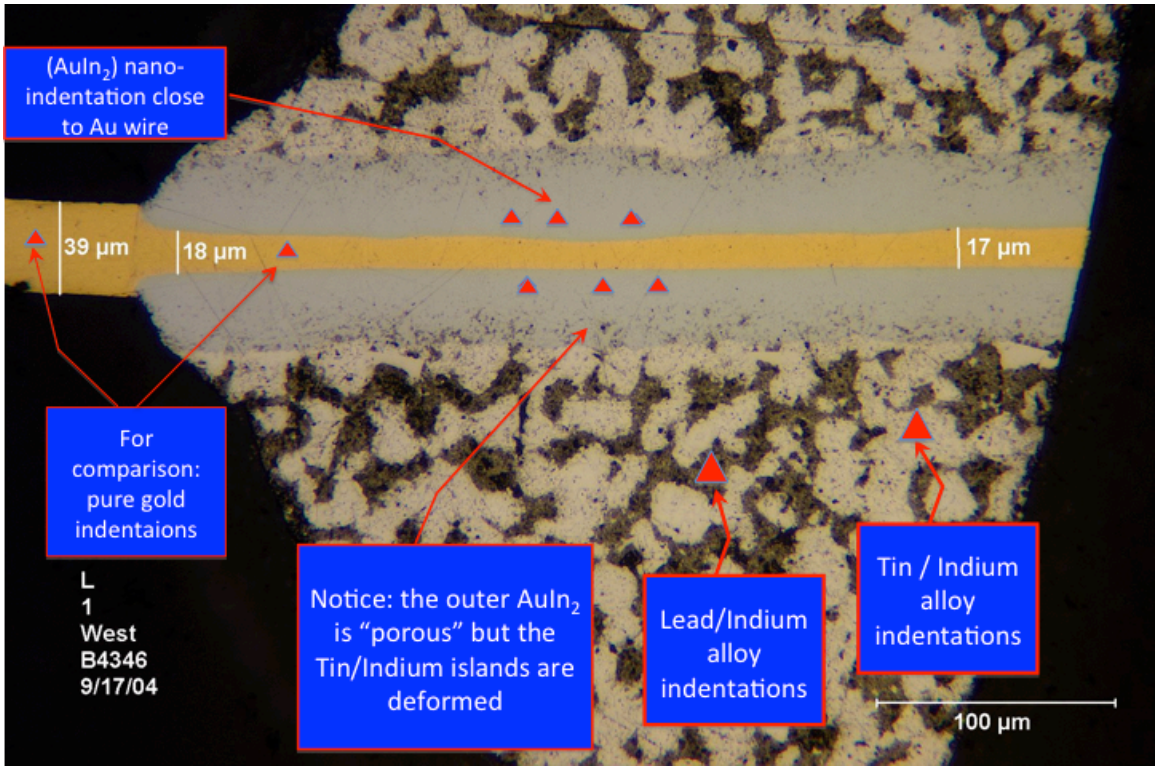

Figure 19. Location of nano-indentation on an axial section 1.5 mil gold-wire in a solder mound.

To determine mechanical properties nano-indentations were made with a Berkowitch diamond tip as shown in figure 19 into gold, $AuIn_2$ close to the gold wire, and into Pb/In and Pb/Sn "grains". $AuIn_2$ locations were chosen close to the gold wire's surface to assure well-formed material. It is evident from figure 19 that the outer $AuIn_2$ layers are either porous or full of Pb/In inclusions, as might be expected from the arguments in section VI.1, since the outermost layer has been stretched to approximately twice the diameter it had when it was initially formed at the skin of the gold wire with approximately 39µm diameter. If the dark pores in the outer $AuIn_2$ layers are filled with Pb/In, it would imply that outer $AuIn_2$ layers crack as the next layer is formed and that the relatively soft Pb/In (see figure 20 below) is squeezed into those cracks by the surrounding solder during the "healing" process. The much harder Sn/In (see figure 20) is clearly NOT incorporated, it is pushed away, and the shapes of the Sn/In grains near the outer surface of the $AuIn_2$ "ring" are different from their shapes in the bulk, indicating that they have been deformed by the constraining bulk of the solder mound as $AuIn_2$ grows. This constraining force is weakest where there is the least bulk, namely where the gold wire exits from the solder mound. One would expect at that location greater porosity of $AuIn_2$ and less Sn/In grain deformation. That is, however, not very evident in figure 19, but more so in figure 22.

Figure 20 summarizes the results of the nano-indentation measurements.

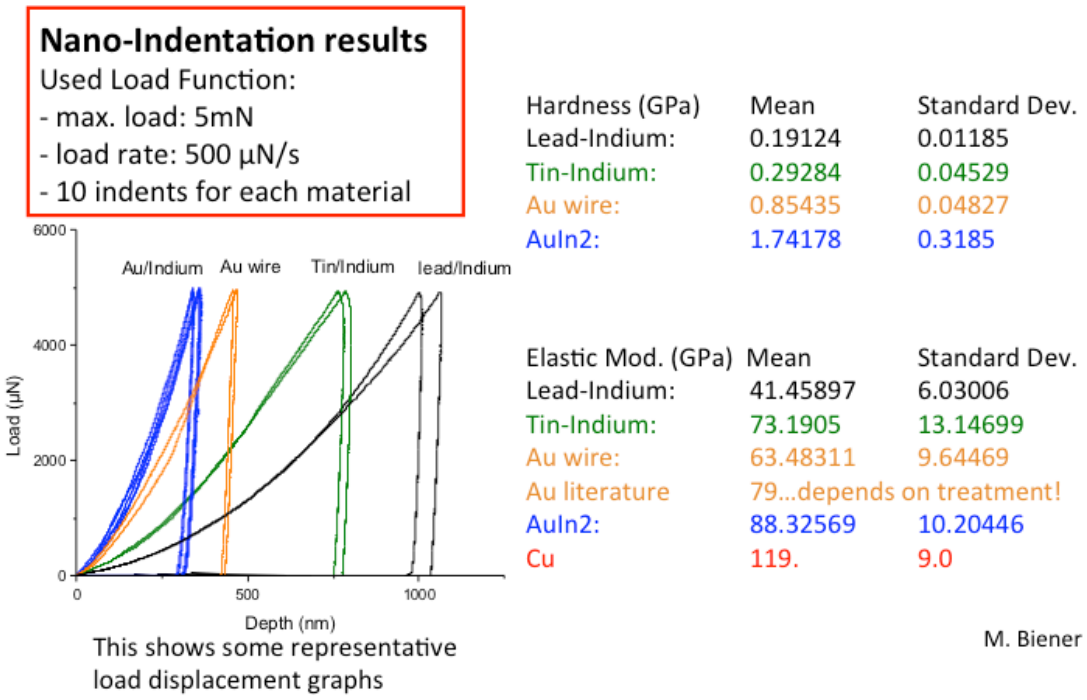

Figure 20. The mechanical properties of Au, AuIn2, Pb/In and Sn/In determined by nano-indentations performed on an axial section of a solder mound. For comparison the literature properties of copper and gold were added.

The hardness of $AuIn_2$ we measure is greater by more than a factor 2 than that measured in reference [2]. $AuIn_2$ has clearly greater hardness and elastic modulus than any other material in the axial section, but it is not as hard (and hence brittle) as glass. It can certainly easily deform Pb/In and even Sn/In. Clearly the strength of the bulk of the solder is needed to accomplish the plastic deformation of $AuIn_2$. That deformation is, however, not guaranteed to be perfect, and hence the growing $AuIn_2$ layer can not be expected to be always integer and free of crack-generated easy diffusion paths that are inconsistent with the application of equation (2).

VIII.3) Physical evidence of imperfect local diffusion control and incomplete plastic deformation of $AuIn_2$ resulting in local "runaway" $AuIn_2$ growth in solder sections and less than theoretical $AuIn_2$ density, respectively.

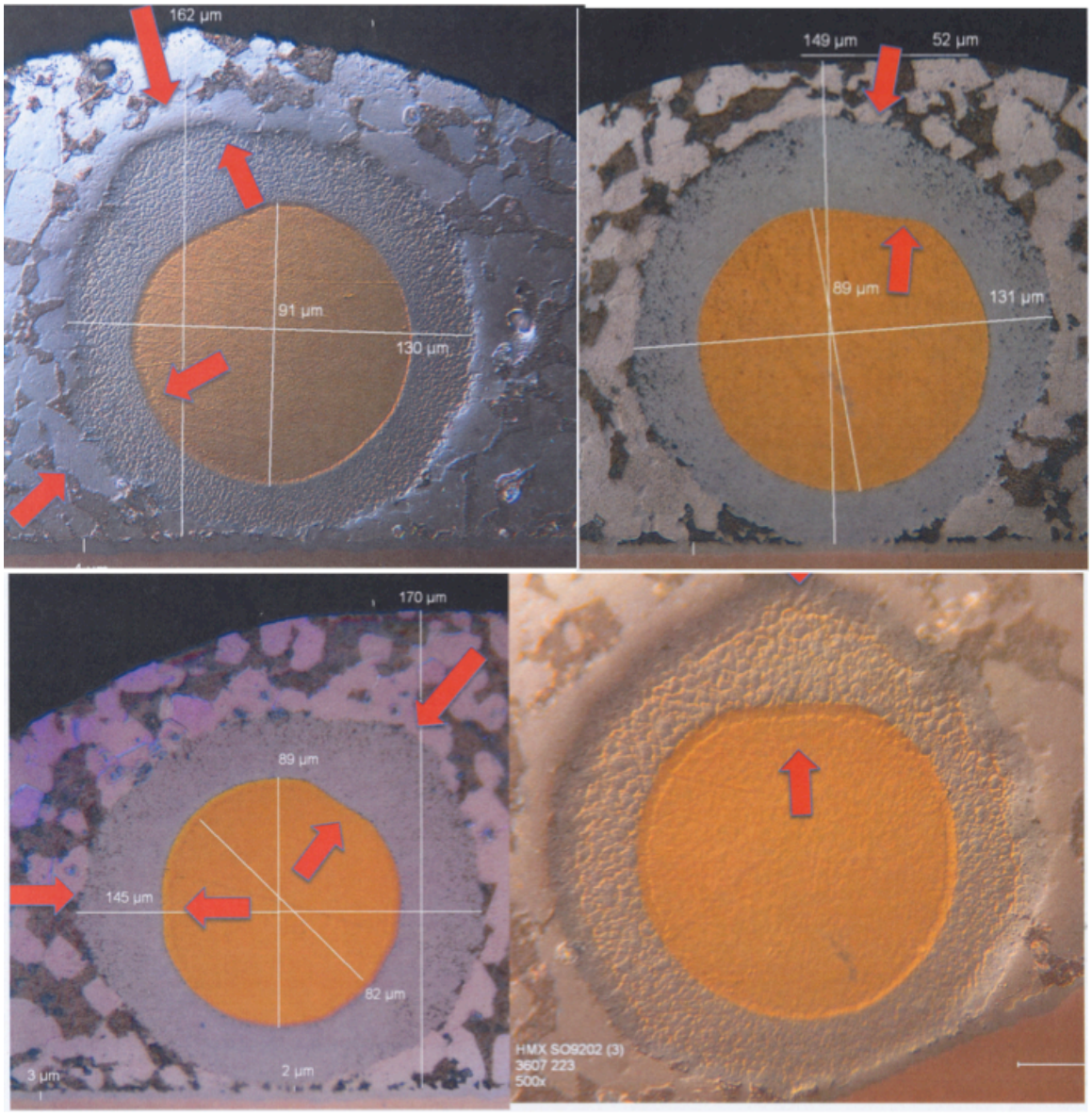

Figure 21. Four cross sections showing "flat spots" on the gold wire with concomitant local increase in gold-indide formation.

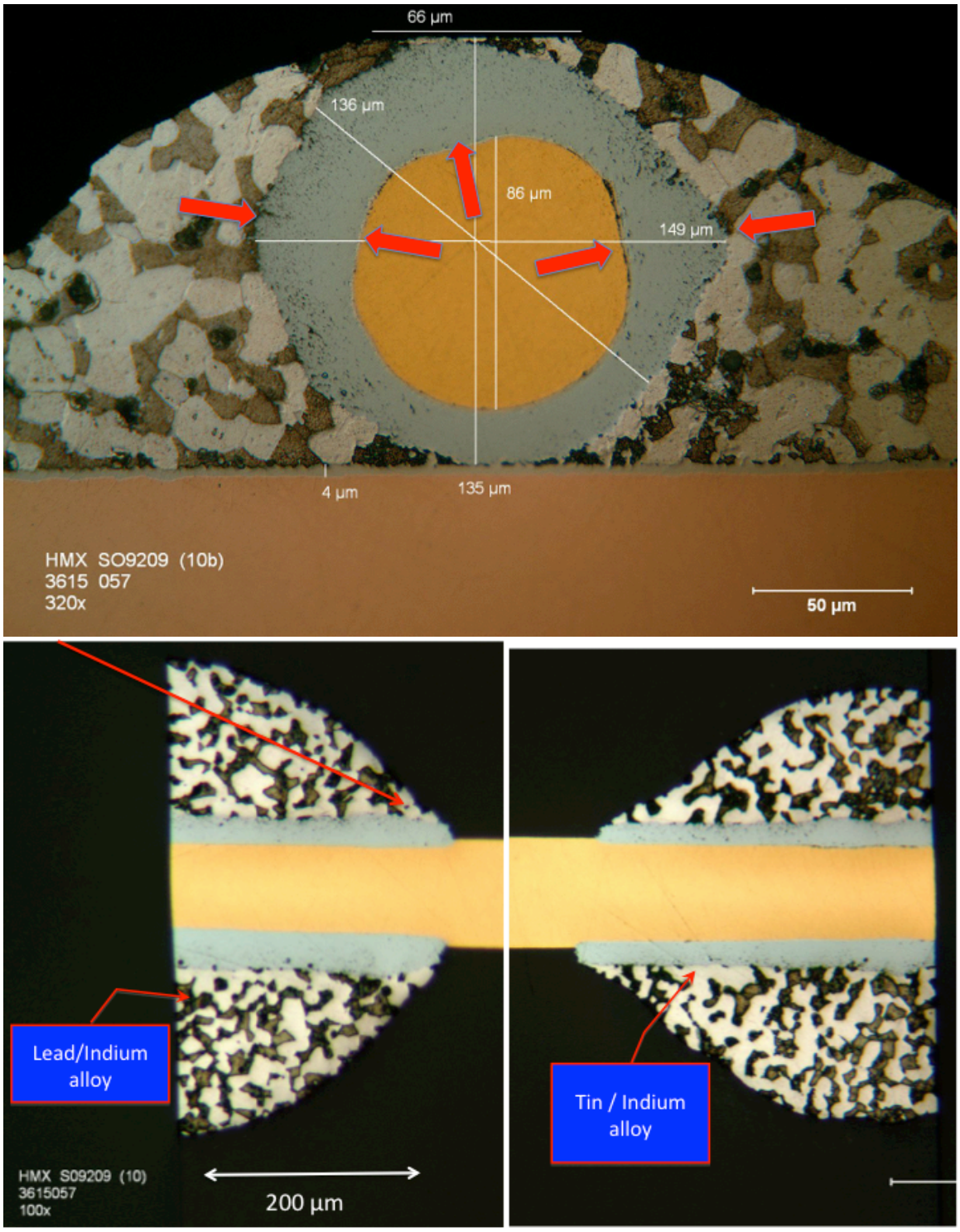

Figure 22. Radial section (upper portion) of a solder mound of one of the sets "33→94" and axial section (lower portion) of a solder mound after accelerated aging.

The radial cross sections of figure 21 and 22 show very clearly that local fast paths of indium transport to the gold surface occur: variations in gold radius loss ("flat spots" on

the gold wire) with concomitant increased $AuIn_2$ formation are quite common. These radial sections are a local "snapshot" of what occurs all along the wire inside the solder mounds. The juxtaposition of a radial section through one solder mound and the axial section (at much lower magnification) through both solder mounds of the same header in figure 22 demonstrates that: there are variations of the $AuIn_2$ and Au diameter all along the wire.

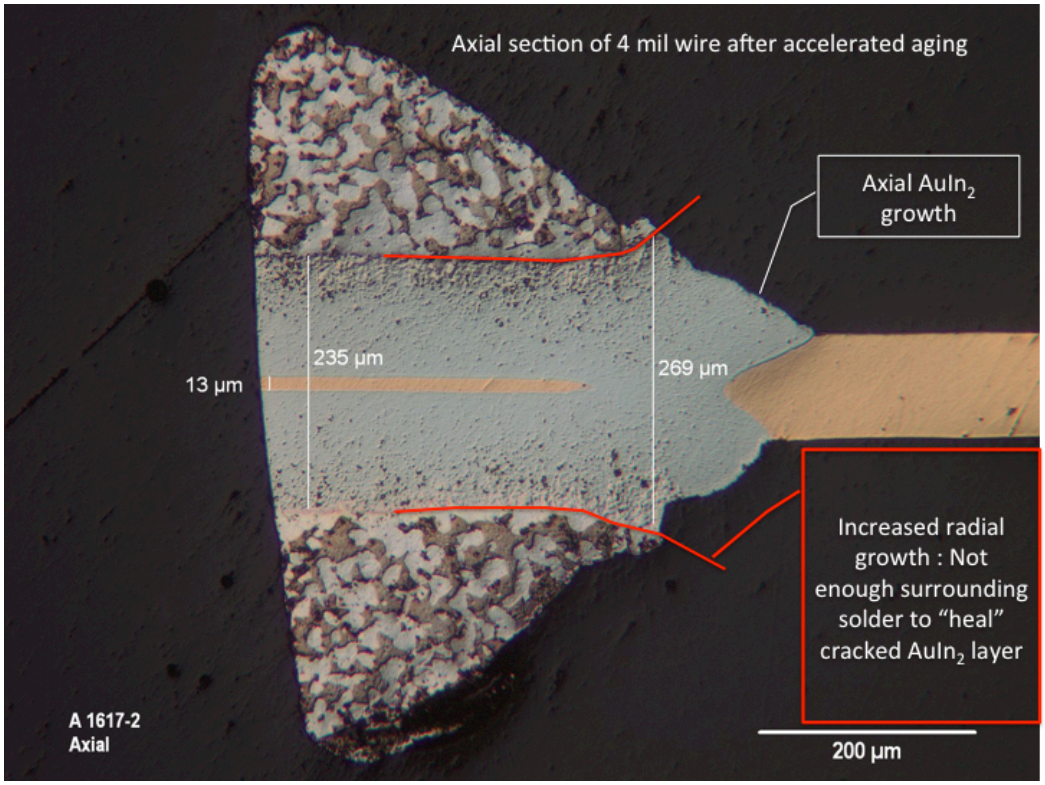

Figure 23. Axial section through one solder mound of a header after accelerated aging at elevated temperature to a gold loss of $\Delta R=(101.6-13)/2= 44.3$ µm.

Figure 23 shows the incomplete plastic deformation-healing and resulting porosity of the $AuIn_2$ layer *inside* the solder mound and, more pronounced, *at the exit point* of the gold wire from the solder mound, where the strength of the surrounding solder is weak, resulting in "bull-nose" formation. The measured $AuIn_2$ and Au diameters shown can be used to calculate the deviation of the measured volume of the $AuIn_2$ layer from the volume expected from its theoretical density ($\rho AuIn_2=10.23$ g/cm^3 [5]). Using the density of gold ($\rho Au=19.3$ g/cm^3) one can readily calculate that a unit volume of Au results in 4.2 unit volumes of $AuIn_2$, and that the expected cross sectional area of $AuIn_2$ is given by

[5] Gmelin, Handbuch der Anorg. Chem. Vol. 62, p. 831. Verlag Chemie 1954. E. Zintl, A. Harder, and W. Haucke, Z Phys Chem B-Chem E **35** (1937).

$AuIn_2AreaExpected = (4.2*(\pi/4)*(OriginalAuDiameter-MeasuredAuDiameter^2)$ (5)

$= 33493.3\ \mu m\text{^}2$

while the measured cross sectional area of $AuIn_2$ is

$AuIn_2AreaMeasured = (\pi/4)*(AuIn_2Diameter^2-MeasuredAuDiameter^2)$ (6)

$= 43240.9\ \mu m^2$

Hence, the $AuIn_2$ formed inside the solder mound is not completely plastically deformed during its growth, it has, *on average*, only about 78% of its theoretical density; its density is even less at the exit of the gold wire from the solder mound. Therefore local deviations from diffusion-controlled growth must be expected.

IX.) Summary and Conclusion

The diffusion control model applied to the actual time/temperature history is shown to fit the experimentally observed gold radius loss ΔR of a set of 4 mil headers of widely varying temperature histories very well, always within the measuring error. A functional dependence $\sum(\Delta R)$ of the standard deviation $\sum$ on the magnitude of the average radius loss ΔR is deduced from $\sum$ values of existing ΔR data sets of 1.5 mil wires together with the $\sum$ values of this 4 mil wire set. This $\sum(\Delta R)$ functional dependence is tested on the scatter of data measured on 1.5 mil wires held at temperature for approximately 30 years, and found to be consistent with those measurements. The diffusion control model together with the $\sum(\Delta R)$ function is used to predict ΔR, $\Delta R \pm \sum$, $\Delta R \pm 2\sum$, $\Delta R \pm 3\sum$ for times up to 100 years.
The maximum expected gold radius loss $\Delta R+3\sum$ is predicted to be 24μm at age 100 years.

Local deviations from diffusion control caused by imperfections in the $AuIn_2$ layer are shown to be expected in circular geometry, and documented in a number of radial and axial cross sections of solder mounts of this set of 4 mil headers. The average density of the $AuIn_2$ layer inside the solder mound is shown to be about 25% less than its theoretical density, indicating incomplete “healing” of cracks in the expanding AuIn2 layer by the surrounding solder.

The hardness and elastic modulus of $AuIn_2$ and of Pb/In and Sn/In grains have been determined by nano-indentation.

The appendix shows that Millares’s equations leads to almost the same results as the diffusion-control model. This close agreement of two models based on different data sets suggests strongly that the gold loss in the low temperature range of interest can be predicted with confidence.

II) Appendix.

Comparison between Millares's model and the LLNLdiffusion-control model.

In the introduction it was pointed out that Millares [3] has independently developed from measurements of the reaction of gold with indium in planar geometry above 50°C a model that combines the linear and diffusion controlled reaction. Millares postulates that at all times the total time needed to form $AuIn_2$ is determined by adding the time that indium atoms needs to diffuse towards the gold surface through the $AuIn_2$ layer to the time needed at the gold surface to form $AuIn_2$, resulting in the equation

$$\text{Reaction time } t_{reaction} = x^2/K_p + x/K_1 \qquad (7)$$

Where x is the thickness of the $AuIn_2$ layer. After converting $AuIn_2$ thickness to gold thickness lost, polynomials of the form $t_{reaction} = A + B*x + C*x^2$ were fit to Millares' data at *all* his data plotted as "Time, Month" versus "Measured Gold Loss X, µm". An example is shown in figure 24 for data at 100°C. Not all fits produced as credible a fit. In that way "Kp^-1AuMonthPolynomialFit" and "K1^-1AuMonthPolynomialFit" were deduced.

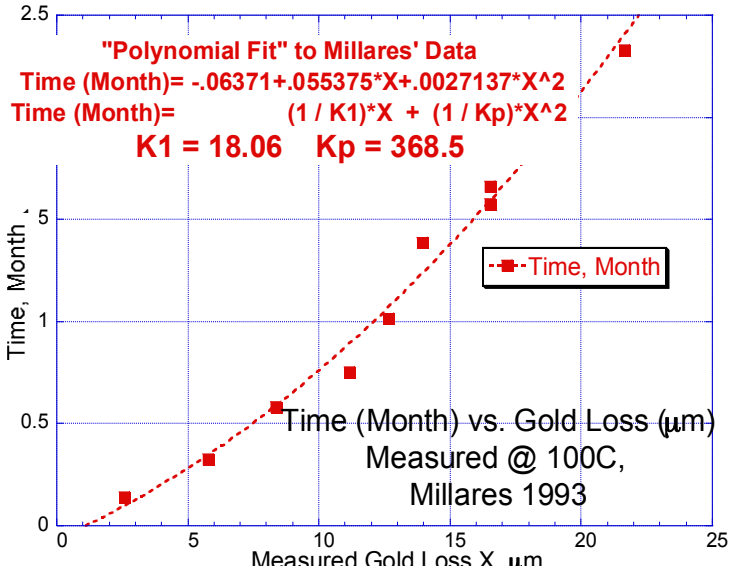

Figure 24. A polynomial fit to Millares' data at 100°C.

In the same way "K_p^-1AuMonthLLNL"+ "K_1^-1MonthLLNL" values can be defined for the linear and diffusion-control model discussed in part III for the regimes in which they are valid, as discussed in detail in reference [2].

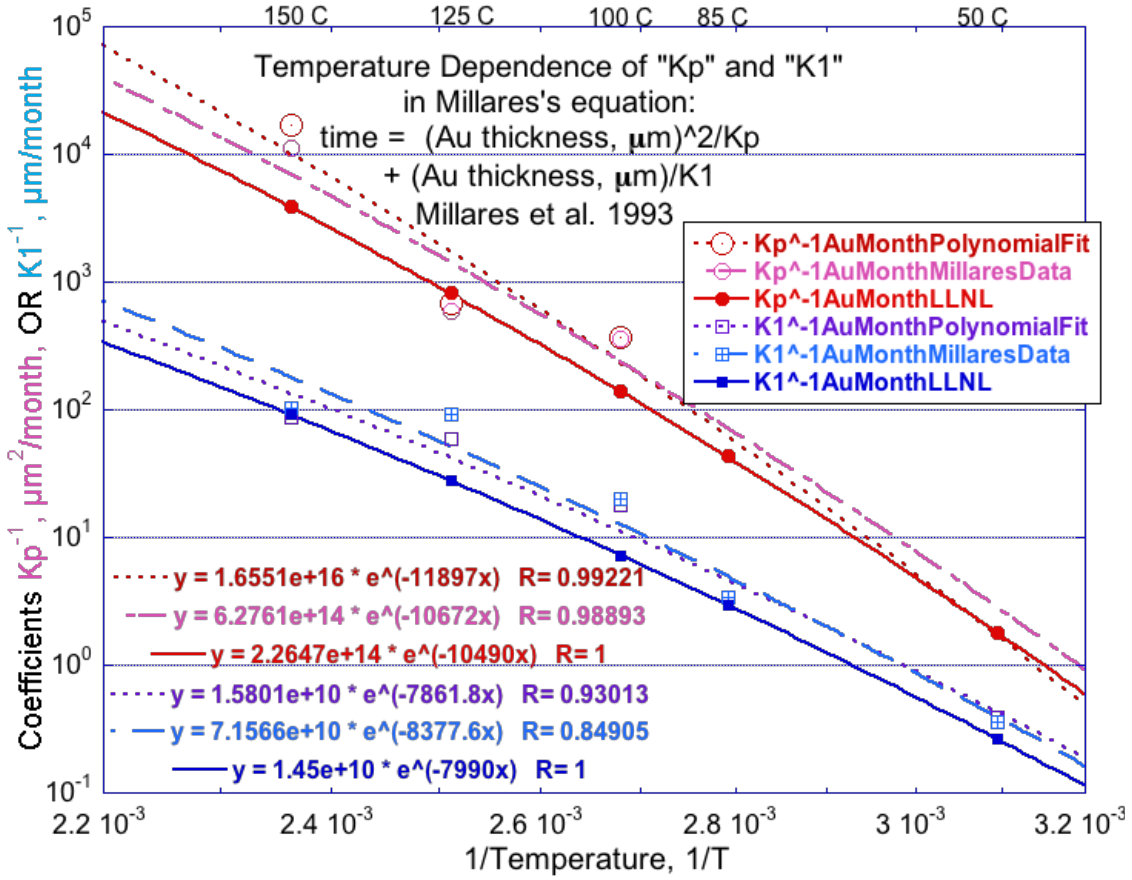

Figure 25. A plot of Millares' fit to his data called "Kp^-1AuMonthMillaresData" and "K1^-1AuMonthMillaresData" as published, our fits to Millares' data called "Kp^-1AuMonthPolynomialFit" and "K1^-1AuMonthPolynomialFit", plus "K_p^-1AuMonthLLNL" and "K_1^-1MonthLLNL" versus inverse temperature, together with exponential fits to all pairs.

In figure 25 exponential fits are derived to allow extrapolation of Millares' work to lower temperatures. With these exponential functions for Kp and K1 one can calculate the gold loss ΔR as a function of time (month) for temperatures below 50°C,

$$\Delta R = \sqrt{[time * Kp + (Kp/2K1)^2]} - (Kp/2K1) \qquad (8)$$

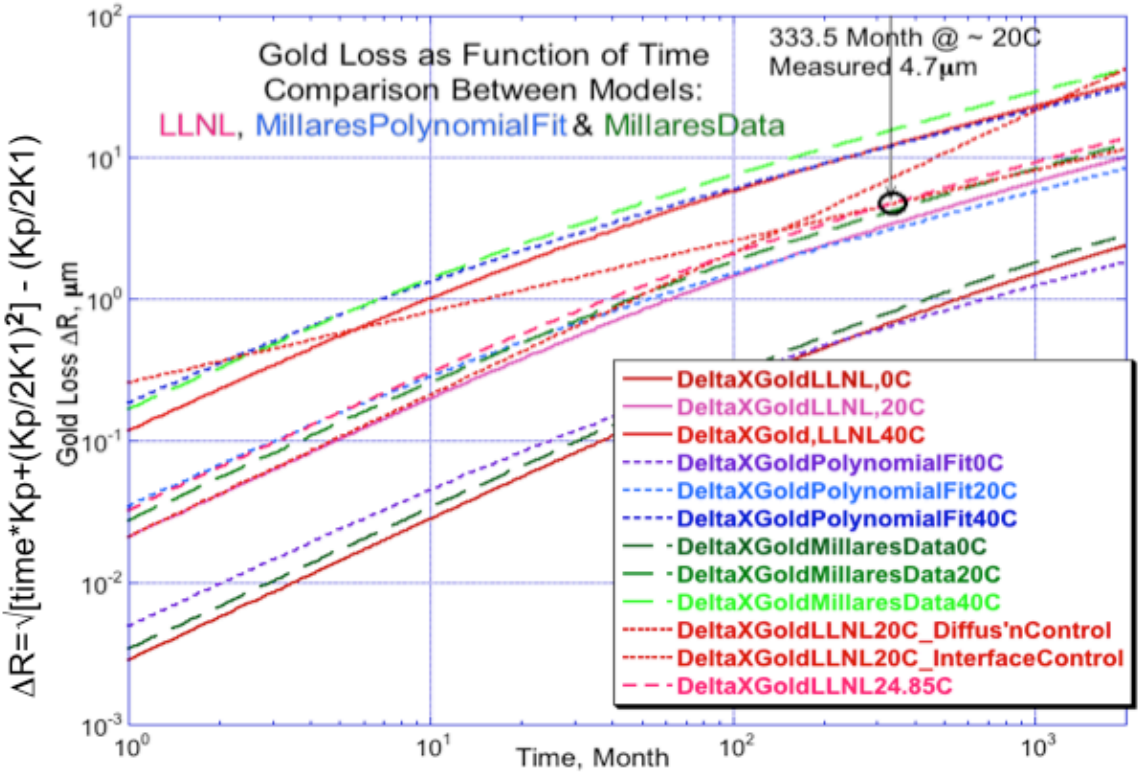

Figure 26. The first 9 lines in the box and their corresponding curves are the gold radius losses ΔR calculated using equation (8), employing *both* K1 and Kp equations derived in figure 25 even for "DeltaXGoldLLNL" in the upper three lines in the box, where K1 and Kp each should only be used in its appropriate range, as described in reference [2]. Consequently curves corresponding to those upper three lines *underestimate* the gold loss ΔR. The first two of the last three lines use in equation (8) for "DeltaXGoldLLNL" only either the value of K1(linear with time) or Kp (proportional to √time) at 20°C. The corresponding dotted red lines intersect at times above 100 month where the reaction becomes diffusion-controlled. The curve corresponding to "Diffus'nControl" matches the measured ΔR value of the "storage set" of part II.1.) at 333.5 month, as in part III.2.). The "green" curve "DeltaXGoldMillaresData20C" based on the extended exponential fit of the K1 and Kp values published by Millares is only slightly below the measured ΔR=4.7µm value of the storage set. The "blue" curve at 20C based on our polynomial fit to the Millares data is lower than ΔR=4.7µm. at 333.5 month.

In summary, here is what figure 26 shows: 1) all models show a slope of ½, i.e. diffusion control after about 100 month, which is used in the LLNL "diffusion control" model. 2) using extensions of Millares' published K1 and Kp values to lower temperatures produces at 20°C a ΔR value close to what is observed experimentally.
This close agreement of two models based on different data sets suggests strongly that the gold loss in the low temperature range of interest can be predicted with confidence.